

# Homogenization of the fluid-saturated piezoelectric porous media<sup>☆</sup>

E. Rohan<sup>a,\*</sup>, V. Lukeš<sup>a</sup>

<sup>a</sup>*Department of Mechanics & NTIS New Technologies for Information Society, Faculty of Applied Sciences, University of West Bohemia in Pilsen, Univerzitní 22, 30100 Plzeň, Czech Republic*

---

## Abstract

The paper is devoted to the homogenization of porous piezoelectric materials saturated by electrically inert fluid. The solid part of a representative volume element consists of the piezoelectric skeleton with embedded conductors. The pore fluid in the periodic structure can constitute a single connected domain, or an array of inclusions. Also the conducting parts are represented by several mutually separated connected domains, or by inclusions. Two of four possible arrangements are considered for upscaling by the homogenization method. The macroscopic model of the first type involves coefficients responsible for interactions between the electric field and the pore pressure, or the pore volume. For the second type, the electrodes can be used for controlling the electric field at the pore level, so that the deformation and the pore volume can be influenced locally. Effective constitutive coefficients are computed using characteristic responses of the microstructure. The two-scale modelling procedure is implemented numerically using the finite element method. The macroscopic strain and electric fields are used to reconstruct the corresponding local responses at the pore level. For validation of the models, these are compared with results obtained by direct numerical simulations of the heterogeneous structure; a good agreement is demonstrated, showing relevance of the two-scale numerical modelling approach.

*Keywords:* multiscale modelling, piezoelectric material, porous media, homogenization

---

<sup>☆</sup>Preprint submitted to Elsevier.

\*Corresponding author.

*Email addresses:* rohan@kme.zcu.cz (E. Rohan), vlukes@kme.zcu.cz (V. Lukeš)

---

## 1. Introduction

The piezoelectric effects which couple the mechanical deformation and the electrical field have been studied since the middle of eighteenth century, however the piezoelectric materials became widespread during the World War I due to their use in resonators for detecting the acoustic sources produced by submarines using echolocation. After the World War II, apart of quartz, new types of the piezoelectric materials, such as barium titanite ( $BaTiO_3$ ) and other synthesizes piezoceramic materials were developed with their dielectric constants much higher than those found in natural piezoelectric materials, such as quartz and some other minerals, or bone. Since then, the piezoelectric materials have found vast applications in electronics, mechatronics, and micro-system technology, being extensively used in the design of transducers, sensors and energy harvesters. Smart structures, such as microelectromechanical systems (MEMS) based on these materials allow for intelligent self-monitoring and self-control capabilities. Nowadays the piezoelectric sensor-actuator systems can be distributed continuously, being attached to the surface of other structural parts. Such an arrangement can be used *e.g.* in the aerospace industry to control vibrations, or acoustic radiation of thin flexible structures.

For modelling periodically heterogeneous media with piezoelectric components, classical upscaling techniques has been employed. Besides the micromechanics approaches including the Mori-Tanaka and self consistent upscaling schemes, [1], the classical periodic homogenization based on the formal two-scale asymptotic expansion method [2, 3], or on the two-scale convergence [4] and the periodic unfolding method [5] has been used. Recently, the homogenization of thermoelectric materials was treated in [6]. Homogenization of the periodic composites consisting of piezoelectric matrix and elastic anisotropic inclusions accounting for bone cells was described in [7]; therein it has been suggested to exploit the piezoelectric effect in the design of a new type of bio-materials which should assist in bone healing and regeneration. Such possible application for piezoelectric materials in biomedical engineering is motivated by the electrochemical processes in biological tissues, which are coupled tightly with periodic mechanical loading assisted by the electric field. Performance of the tissue regeneration and remodelling may be enhanced by activated bio-piezo porous implants which can accel-

erate these processes undergoing at the microscopic level and related to the electro-mechanical transduction, cf. [8, 9]. The Suquet method of homogenization has been used to obtain analytic models of particulate and fibrous piezoelectric composites [10]. Apart of the homogenization of heterogeneous piezoelectric media, an asymptotic analysis has been applied to derive higher order models of piezoelectric rods and beams, starting from the 3D piezoelectricity problem [11].

In [12], the shape sensitivity formulae were derived for a class of 2D microstructures comprising one piezoelectric and one arbitrary elastic material, whereby the shape of the interface between the two materials was parameterized. As a challenge for the material design, the numerical tests have shown how a suitable geometry of the interface can amplify some of the homogenized coefficients, namely the third-order tensors associated with the electromechanical coupling. Sensitivity of the effective medium properties to the microstructure properties were also reported in [13].

Besides the periodic homogenization, in [1], the Mori-Tanaka and the self-consistent schemes were used for upscaling the drained porous piezoelectric materials. Concerning the fluid saturated porous piezoelectric media, the asymptotic method has been applied in [14] to derive macroscopic constitutive laws accounting for the fluid-structure interaction at the pore level, whereby a simplified model of electrolytes was considered. In the context of the bone tissue biomechanics, the macroscopic influence of piezoelectric effects observable in dried bone was studied in [15] using the homogenization approach.

Propagation of electroacoustic waves in an reinforced piezoelectric medium was treated in [16]. The low frequency acoustic wave propagation in the porous piezoelectric materials has been subject of several works [17, 18, 19, 20]. In these papers, the modelling is based on the Biot theory of porous media elaborated within the phenomenological approach, therefore, influences of specific microstructures on the wave dispersion have not been studied yet.

This paper is focused on the derivation of the effective material coefficients of the fluid-saturated porous media with the piezoelectric skeleton using the homogenization framework. A related topic was treated recently in [10], where a special type of piezoelectric anisotropic composite materials was studied using numerical and analytical methods. Although the porosity influence was examined and the figures of merit related to the hydrostatic strain coefficient were also investigated, we pursue another homogenization approach which is based on the periodic homogenization of the static fluid-

structure interaction, as reported in [21] in the context of the hierarchical porous poroelastic media, cf. [22]. We assume a quasistatic loading, such that inertia and viscosity related effects can be neglected. As the consequence, in any connected porosity, a unique pressure is established which satisfies the equilibrium. Using the homogenization of the fluid-structure interaction problem at the microscopic scale, we obtain macroscopic models of the upscaled piezo-poroelastic medium for different periodic microstructures; one connected porosity, or an array of fluid filled inclusions is combined with piezoelectric skeleton which can contain mutually separated conductors (metallic parts). We consider two different situations: 1) the conductors are distributed as a periodic arrays of mutually separated inclusions, or 2) the conducting parts constitute two or more electrodes such that each of these electrodes presents a connected porous structure. In the second case, different electric potential is prescribed to different electrodes, so that electric fields induced in the microstructure can be controlled.

The paper is organized as follows. In Section 2, different microscopic configurations of the periodic porous piezoelectric medium are defined and the model equations are introduced, yielding the weak formulation. The homogenization of the static fluid-structure interaction is reported in Sections 3 and 4, for the two above mentioned designs of the conducting parts. In both these sections, the local problems for the characteristic responses of the representative period cell are derived and the homogenized effective material coefficients are obtained. These are involved in the macroscopic equations governing behaviour of the upscaled poro-piezoelectric medium. Using the characteristic responses and the macroscopic fields, the displacement, pressure and electric fields can be reconstructed at the microscopic level, as reported in Section 6. Finally, in Section 7, we present numerical illustration of the derived macroscopic models. For validation of these models, direct numerical simulation of the heterogeneous media are compared with the responses computed using the homogenized problems. Some technical supporting material is explained in the Appendix.

*Some basic notations.* In the paper, the mathematical models are formulated in a Cartesian framework of reference  $\mathcal{R}(O; \mathbf{e}_1, \mathbf{e}_2, \mathbf{e}_3)$  where  $O$  is the origin of the space and  $(\mathbf{e}_1, \mathbf{e}_2, \mathbf{e}_3)$  is a orthonormal basis for this space. The coordinates of a point  $M$  are specified by  $x = (x_1, x_2, x_3)$  in  $\mathcal{R}$ . The boldface notation for vectors,  $\mathbf{a} = (a_i)$ , and for tensors,  $\mathbf{b} = (b_{ij})$ , is used. The following special notation is used for the electric field  $\vec{E}$ , and the electric

displacement vector  $\bar{D}$ . Furthermore, a special notation is introduced for the 3rd order tensors associated with piezoelectric coupling,  $\underline{\mathbf{G}}^H, \underline{\mathbf{g}}$ . The gradient and divergence operators are respectively denoted by  $\nabla$  and  $\bar{\nabla}$ . When these operators have a subscript which is space variable, it is for indicating that the operator acts relatively at this space variable, for instance  $\nabla_x = (\partial_i^x)$ . The small strain tensor is denoted by  $\mathbf{e}(\mathbf{u}^\varepsilon) = (\nabla \mathbf{u}^\varepsilon + (\nabla \mathbf{u}^\varepsilon)^T)/2$ . The symbol dot ‘ $\cdot$ ’ denotes the scalar product between two vectors and the symbol colon ‘ $:$ ’ stands for scalar (inner) product of two second-order tensors. Throughout the paper,  $x$  denotes the global (“macroscopic”) coordinates, while the “local” coordinates  $y$  describe positions within the representative unit cell  $Y \subset \mathbb{R}^3$  where  $\mathbb{R}$  is the set of real numbers. By  $dV$  (or  $dV_x$ ) and  $dV_y$  we denote the elementary volume elements associated with coordinates  $x$  and  $y$ , respectively, while  $dV_{xy}$  is the elementary volume in a cross-product domain  $\Omega \times Y$ . Accordingly, elementary surfaces are designated by  $dS$ ,  $dS_x$  and  $dS_y$ .

By  $\bar{f}_{Y_d} = |Y|^{-1} \int_{Y_d}$  with  $Y_d \subset \bar{Y}$  we denote the local average. The Lebesgue spaces of 2nd-power integrable functions on a domain  $D$  is denoted by  $L^2(D)$ , the Sobolev space  $\mathbf{W}^{1,2}(D)$  of the square integrable vector-valued functions on  $D$  including the 1st order generalized derivative, is abbreviated by  $\mathbf{H}^1(D)$ . The unit normal vector outward to domain  $D_s$  is denoted by  $\mathbf{n}^{[s]}$ .

## 2. Microscopic model of porous piezoelectric media

There are typically two characteristic lengths:  $\ell$  describes the heterogeneity size and  $L$  is the relevant macroscopic size. The ration  $\varepsilon = \ell/L$  is called the scale parameter. As usually, we consider material properties of the heterogeneous medium oscillating with period  $\ell$  relative to the spacial position. The asymptotic method of homogenization is based on the asymptotic analysis of the mathematical model for  $\varepsilon \rightarrow 0$ .

### 2.1. Periodic microstructure

The medium is generated by copies of the representative volume element (RVE)  $Z^\varepsilon \subset \mathbb{R}^3$  as a periodic lattice, so that  $\varepsilon a_k$  is the lattice period in the  $k$ -th coordinate direction. For the “real size” RVE, we introduce its rescaled copy  $Y = \varepsilon^{-1} Z^\varepsilon$  which is called the rescaled elementary periodic cell  $Y$  defined by  $Y = \prod_{i=k}^3 ]-a_k/2, a_k/2[$ ; typically  $|Y| = 1$ , see Fig. 1. In this paper we consider  $a_k = 1$  without loss of generality. For any given  $\varepsilon > 0$  we define mesoscopic (zoomed) coordinates  $y = (y_k) \in Y$  which for a given “macroscopic” position  $x$  are given by the localization function  $\mathcal{Y} : x \mapsto y$

defined by:  $y_k = \mathcal{Y}_k(x) = (x_k - \varepsilon a_k \text{int} \{x_k / (\varepsilon a_k)\}) / \varepsilon$  for  $k = 1, 2, 3$ , where  $\text{int} \{z\}$  denotes the integer part of  $z$ .

## 2.2. Porous piezoelectric solid saturated by static fluid

We consider a quasi-static loading of a piezoelectric skeleton interacting with a viscous fluid saturating pores in the skeleton.

The piezo-poroelastic medium occupies an open bounded domain  $\Omega \subset \mathbb{R}^3$  with Lipschitz boundary  $\partial\Omega$ . The following decomposition of  $\Omega$  into the piezoelectric matrix,  $\Omega_m^\varepsilon$ , elastic conductive inclusions,  $\Omega_*^\varepsilon$ , and fluid-saturated channel parts,  $\Omega_c^\varepsilon$ , is considered:

$$\begin{aligned} \Omega &= \Omega_c^\varepsilon \cup \Omega_m^\varepsilon \cup \Omega_*^\varepsilon, \quad \Omega_c^\varepsilon \cap \Omega_m^\varepsilon \cap \Omega_*^\varepsilon = \emptyset, \\ \text{where } \Omega_*^\varepsilon &= \bigcup_k \Omega_*^{k,\varepsilon}. \end{aligned} \quad (1)$$

By  $\Gamma_c^\varepsilon$  we denote the solid-fluid interface,  $\Gamma_c^\varepsilon = \overline{\Omega_m^\varepsilon \cup \Omega_*^\varepsilon} \cap \overline{\Omega_c^\varepsilon}$ . The interface between the piezoelectric matrix and the conductors  $\Gamma_*^\varepsilon$  consists of its subparts  $\Gamma_*^{k,\varepsilon}$  introduced, as follows:

$$\Gamma_*^\varepsilon = \partial\Omega_*^\varepsilon \cap \overline{\Omega_m^\varepsilon} \quad \text{and} \quad \Gamma_*^{k,\varepsilon} = \partial\Omega_*^{k,\varepsilon} \cap \overline{\Omega_m^\varepsilon}. \quad (2)$$

Further we denote by  $\partial_{\text{ext}}\Omega_m^\varepsilon = \overline{\Omega_m^\varepsilon} \cap \partial\Omega$  the exterior boundaries of  $\Omega_m^\varepsilon$ . In analogy, we define  $\partial_{\text{ext}}\Omega_*^\varepsilon$  and  $\partial_{\text{ext}}\Omega_c^\varepsilon$  as the exterior parts on the boundaries of the conductive solid  $\Omega_*^\varepsilon$  and the fluid  $\Omega_c^\varepsilon$ , respectively. We assume that  $\Omega_m^\varepsilon$  is connected domain, however  $\Omega_c^\varepsilon$  may consists of disconnected inclusions; the latter option will be considered as a special case. The conductive material is distributed as a connected phase for each index  $k$ , such that  $\Omega_*^{k,\varepsilon}$  is connected.

As we often refer to the solid part consisting of the piezoelectric matrix and the conductor part, we introduce  $\Omega_{m*}^\varepsilon = \Omega_m^\varepsilon \cup \Omega_*^\varepsilon \cup \Gamma_*^\varepsilon$ , recalling the interface  $\Gamma_*^\varepsilon$  between the two parts is defined in (2). The boundary conditions are prescribed on the external boundary  $\partial_{\text{ext}}\Omega_{m*}^\varepsilon = \partial\Omega_{m*}^\varepsilon \setminus \Gamma_*^\varepsilon$  involving both the solid phases; the following two splits are defined,  $\partial_{\text{ext}}\Omega_{m*}^\varepsilon = \Gamma_{\mathbf{u}}^\varepsilon \cup \Gamma_\sigma^\varepsilon$  and  $\partial_{\text{ext}}\Omega_{m*}^\varepsilon = \Gamma_\varphi^\varepsilon \cup \Gamma_{\bar{D}}^\varepsilon$  such that

$$\Gamma_\sigma^\varepsilon = \partial_{\text{ext}}\Omega_{m*}^\varepsilon \setminus \Gamma_{\mathbf{u}}^\varepsilon \quad \text{and} \quad \Gamma_{\bar{D}}^\varepsilon = \partial_{\text{ext}}\Omega_{m*}^\varepsilon \setminus \Gamma_\varphi^\varepsilon. \quad (3)$$

To respect spatial fluctuations of the material parameters, by virtue of the scale parameter introduced above, all material coefficients and unknown functions involved in the mathematical model which depend on the scale

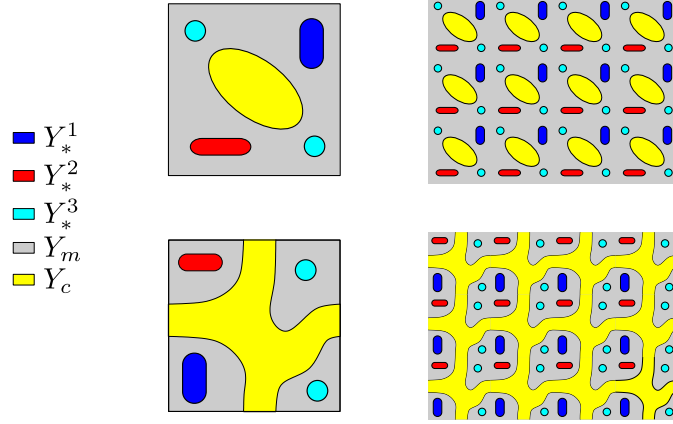


Figure 1: The scheme of the representative periodic cell decomposition and the generated periodic structure. Two configuration of the porous microstructure with conducting parts  $Y_*^k$  embedded in the solid piezoelectric skeleton  $Y_m$ .

will be labeled by superscript  $\varepsilon$ . In the piezoelectric solid, the Cauchy stress tensor  $\boldsymbol{\sigma}^\varepsilon$  and the electric displacement  $\vec{D}^\varepsilon$  depend on the strain tensor  $\mathbf{e}(\mathbf{u}^\varepsilon) = (\nabla \mathbf{u}^\varepsilon + (\nabla \mathbf{u}^\varepsilon)^T)/2$  defined in terms of the displacement field  $\mathbf{u}^\varepsilon = (u_i^\varepsilon)$ , and on the electric field  $\vec{E}^\varepsilon = \nabla \varphi^\varepsilon$  defined in terms of the electric potential  $\varphi^\varepsilon$ . The following constitutive equations characterize the piezoelectric solid in  $\Omega_m^\varepsilon$ ,

$$\begin{aligned} \sigma_{ij}^\varepsilon(\mathbf{u}^\varepsilon, \varphi^\varepsilon) &= A_{ijkl}^\varepsilon e_{kl}^\varepsilon(\mathbf{u}^\varepsilon) - g_{kij}^\varepsilon E_k^\varepsilon(\varphi^\varepsilon), \\ D_k^\varepsilon(\mathbf{u}^\varepsilon, \varphi^\varepsilon) &= g_{kij}^\varepsilon e_{ij}^\varepsilon(\mathbf{u}^\varepsilon) + d_{kl}^\varepsilon E_l^\varepsilon(\varphi^\varepsilon), \end{aligned} \quad (4)$$

where  $\mathbb{A}^\varepsilon = (A_{ijkl}^\varepsilon)$  is the elasticity fourth-order symmetric positive definite tensor of the solid, where  $A_{ijkl} = A_{klij} = A_{jilk}$ , the deformation is coupled with the electric field through the 3rd order tensor  $\underline{\mathbf{g}}^\varepsilon = (g_{kij}^\varepsilon)$ ,  $g_{kij}^\varepsilon = g_{kji}^\varepsilon$  and  $\underline{\mathbf{d}} = (d_{kl})$  is the permittivity tensor. The conductive solid is described by its elasticity  $\mathbb{A}^\varepsilon$  only. The permittivity in  $\Omega_*^{k,\varepsilon}$  is infinitely large, so that we assume  $\varphi^\varepsilon = \bar{\varphi}^k$ .

In this paper we shall use a compact (global) notation, such that (4) can be written (we drop the superscript  $\varepsilon$  for the moment),  $\boldsymbol{\sigma} = \mathbb{A} \mathbf{e}(\mathbf{u}) - \underline{\mathbf{g}}^T \cdot \vec{E}(\varphi)$ , and  $\vec{D} = \underline{\mathbf{g}} : \mathbf{e}(\mathbf{u}) + \underline{\mathbf{d}} \vec{E}$ .

### 2.3. Discussion of possible configurations and the problem formulations

In the context of the steady state – thermodynamic equilibrium under no fluid flow, two situations will be considered, see Fig. 1:

- Case CF – connected porosity (fluid canals)  $\Omega_c^\varepsilon$ : in the thermodynamic equilibrium, the pore fluid pressure is constant (denoted by  $\bar{p}$ );
- Case DF – disconnected fluid inclusions: each  $\Omega_c^{k,\varepsilon}$  is formed by inclusions with diameter  $\approx \varepsilon$ ; such an arrangement admits differences in the fluid pressure associated with neighbouring inclusions.

The first case can be modified for a quasi-static flow in the channels with neglected inertia effects and assuming moderate pressure gradients in the flow, as considered in [22], cf. [23].

Concerning the conductor part, two different configurations are assumed:

- Case D\* – disconnected conductor inclusions: each  $\Omega_*^{k,\varepsilon}$ ,  $k = 1, 2, \dots, \bar{k}^\varepsilon$  is formed by inclusions with diameter  $\approx \varepsilon$ , thus, the  $k$ -th inclusion  $\Omega_*^{k,\varepsilon}$  is contained in a copy of  $Z^\varepsilon$ . Obviously, the number of such inclusions depends on  $\varepsilon$ ;
- Case C\* – connected conductor fibres: each  $\Omega_*^{k,\varepsilon}$  is a connected domain, however, they are mutually disconnected. We consider a finite number  $k^*$  of such conductors.

Each of the two cases, D\* and C\*, needs a special treatment with respect to the homogenization  $\varepsilon \rightarrow 0$  which is the subject of Section 3 and 4, respectively.

#### 2.4. Problem formulations

With reference to the notation related to the domain decomposition and the associated parts of the interfaces and the external boundary, as established above, we introduce differential equations, the interface and the boundary conditions governing static behaviour, or steady state behaviour of the porous fluid saturated piezoelectric medium. The boundary value problems (BVPs) are constituted by the following equations involving the  $\mathbf{u}^\varepsilon$ ,  $\varphi^\varepsilon$  and  $p^\varepsilon$ :

- Equilibrium of the stress and electric displacements,

$$\begin{aligned} -\nabla \cdot \boldsymbol{\sigma}^\varepsilon(\mathbf{u}^\varepsilon, \varphi^\varepsilon) &= \mathbf{f}^\varepsilon, & \text{in } \Omega_{m^*}^\varepsilon, \\ -\nabla \cdot \vec{D}^\varepsilon(\mathbf{u}^\varepsilon, \varphi^\varepsilon) &= q_E^\varepsilon, & \text{in } \Omega_m^\varepsilon, \end{aligned} \quad (5)$$

where  $\mathbf{f}^\varepsilon$  is the volume-force and  $q_E^\varepsilon$  is the volume electric charge;



- The fluid mass conservation is presented for the two cases, CF and DF. Inclusions (DF): Let  $\Omega_c^{k,\varepsilon} \subset \Omega_c^\varepsilon$  be the  $k$ -th inclusion, the mass conservation yields

$$\int_{\partial\Omega_c^{k,\varepsilon}} \mathbf{u}^\varepsilon \cdot \mathbf{n}^{[c]} \, dS + \gamma p^{k,\varepsilon} |\Omega_c^{k,\varepsilon}| = 0, \quad \forall k \in \{1, \dots, \bar{k}^\varepsilon\}, \quad (6)$$

where  $\gamma$  is the fluid compressibility.

Canals (CF): In the steady state, the fluid pressure gradient vanishes, so that one pressure value is attained in the whole connected porosity  $\Omega_c^\varepsilon$ . The fluid volume  $-J^\varepsilon$  injected through the boundary  $\partial_{\text{ext}}\Omega_c^\varepsilon$  into the porosity is compensated by the pore inflation and by the fluid compression, so that (6) is replaced by:

$$\int_{\partial\Omega_c^\varepsilon} \mathbf{u}^\varepsilon \cdot \mathbf{n}^{[c]} \, dS + \gamma p^\varepsilon |\Omega_c^\varepsilon| = -J^\varepsilon. \quad (7)$$

In general, the connected porosity admits flow at the global level of the connected porosity  $\Omega_c^\varepsilon$ . In this case, (6) is replaced by

$$\int_{\partial\Omega_c^\varepsilon} q^\varepsilon (\dot{\mathbf{u}}^\varepsilon \cdot \mathbf{n}^{[c]} + \gamma p^\varepsilon + \nabla \cdot \mathbf{w}^\varepsilon) \, dS = 0, \quad (8)$$

where  $\mathbf{w}^\varepsilon$  is the seepage velocity governed by the Stokes flow and the dot means the time derivative. However, in this paper we shall consider stationary problems only, thus, governed by equations (6) or (7).

- Interface conditions:

$$\begin{aligned} \mathbf{n} \cdot \boldsymbol{\sigma}^\varepsilon &= -p^\varepsilon \mathbf{n}, & \text{on } \Gamma_c^\varepsilon, \\ \mathbf{n}^{[m]} \cdot \vec{D}^\varepsilon &= \varrho_E^\varepsilon, & \text{on } \Gamma_{mc}^\varepsilon, \\ \mathbf{n} \cdot [\boldsymbol{\sigma}^\varepsilon] &= 0, & \text{on } \Gamma_*^\varepsilon, \\ [\mathbf{u}^\varepsilon] &= 0, & \text{on } \Gamma_*^\varepsilon, \\ \varphi^\varepsilon &= \bar{\varphi}^k, & \text{on } \Gamma_*^{k,\varepsilon}, \end{aligned} \quad (9)$$

$$\int_{\Gamma_*^k} \mathbf{n} \cdot \vec{D}^\varepsilon \, dS = 0, \quad k = 1, 2, \dots, k^*,$$

where  $\Gamma_{mc}^\varepsilon = \overline{\Omega_m^\varepsilon} \cap \overline{\Omega_c^\varepsilon}$ , and  $\mathbf{n}$  is the unit normal vector on the interface;  $\mathbf{n}^{[m]}$  points outward to  $\Omega_m^\varepsilon$ .

- Boundary conditions:

$$\begin{aligned}
\mathbf{n}^{[m]} \cdot \boldsymbol{\sigma}^\varepsilon &= \mathbf{h}^\varepsilon, & \text{on } \Gamma_\sigma^\varepsilon, \\
\mathbf{n}^{[m]} \cdot \vec{D}^\varepsilon &= \varrho_E^\varepsilon, & \text{on } \Gamma_D^\varepsilon, \\
\mathbf{u}^\varepsilon &= \bar{\mathbf{u}}, & \text{on } \Gamma_u^\varepsilon, \\
\varphi^\varepsilon &= \bar{\varphi}^0, & \text{on } \Gamma_\varphi^\varepsilon,
\end{aligned} \tag{10}$$

where  $\mathbf{h}^\varepsilon$  and  $\varrho_E^\varepsilon$  are the applied surface-forces and the surface electric charge, respectively.

**Remark 2.1.** *Two BVPs will be pursued in what follows:*

1. *Case CFD\*:* the BVP is constituted by (4),(5),(7), (9) and (10) where the constants  $\bar{\varphi}^k$  for  $k = 1, 2, \dots, k^*$  become parts of the solution.
2. *Case DFC\*:* the BVP is constituted by (4),(5),(6), (9) and (10) whereby we shall assume:
  - given values  $\bar{\varphi}^k$  for the finite number on the conductors,  $k = 1, \dots, k^*$ ;
  - vanishing boundary  $\Gamma_\varphi^\varepsilon$ , i.e. no prescribed voltage  $\bar{\varphi}^0$  on the external boundary.

The other combinations, namely CFC\* and DFD\* can be deduced and are left as an exercise for interested readers.

To obtain a priori estimates independently of  $\varepsilon$ , the surface charge distributed on the interfaces  $\Gamma_c^\varepsilon$  must be scaled appropriately by  $\varepsilon$ ; we shall consider  $\varrho_E^\varepsilon = \varepsilon \bar{\rho}_E$  on  $\Gamma_c^\varepsilon$ , where  $o(\bar{\rho}_E) = \varepsilon^0$ , see (17) below.

*Weak formulation.* Since the homogenization procedure is based on the weak formulations, we shall need the following admissibility sets:

$$\begin{aligned}
\mathcal{U}(\Omega_{m*}^\varepsilon) &= \{ \mathbf{v} \in \mathbf{H}^1(\Omega_{m*}^\varepsilon) \mid \mathbf{v} = \bar{\mathbf{u}} \text{ on } \Gamma_u^\varepsilon \}, \\
\mathcal{V}_0(\Omega_m^\varepsilon, \Gamma_S^\varepsilon) &= \{ \varphi \in H^1(\Omega_m^\varepsilon) \mid \varphi = 0 \text{ on } \Gamma_S^\varepsilon \}, \\
\mathcal{V}_*(\Omega_m^\varepsilon, \Gamma_*^\varepsilon) &= \{ \psi \in H^1(\Omega_m^\varepsilon) \mid \psi = \bar{\psi}^k \text{ on } \Gamma_*^{k,\varepsilon}, k = 1, 2, \dots, k^* \}
\end{aligned} \tag{11}$$

where  $\bar{\psi}^k$  is an arbitrary constant for each  $k = 1, 2, \dots, k^*$ . Below we shall consider two situations which we discuss in Remark 2.2; if  $\bar{\psi} := \bar{\varphi}$  is prescribed in the definition of  $\mathcal{V}_*(\Omega_m^\varepsilon, \Gamma_*^\varepsilon)$ , we write  $\mathcal{V}_*(\Omega_m^\varepsilon, \Gamma_*^\varepsilon, \bar{\varphi})$ .

By  $\mathbf{U}_0(\Omega_{m*}^\varepsilon)$  we denote the space of virtual displacements derived from  $\mathbf{U}(\Omega_{m*}^\varepsilon)$  for  $\bar{\mathbf{u}} = \mathbf{0}$ . Further, we shall employ the following sets

$$\begin{aligned} \mathcal{W}_0(\Omega_m^\varepsilon) &= \mathcal{V}_*(\Omega_m^\varepsilon, \Gamma_*^\varepsilon) \cap \mathcal{V}_0(\Omega_m^\varepsilon, \Gamma_\varphi^\varepsilon), \\ \mathcal{W}_*(\Omega_m^\varepsilon, \Gamma_\varphi^\varepsilon, \bar{\varphi}^0) &= \mathcal{V}_*(\Omega_m^\varepsilon, \Gamma_*^\varepsilon) + \hat{\varphi}, \\ \text{where } \hat{\varphi} \in H^1(\Omega_m^\varepsilon), \text{ and } \hat{\varphi} &= \begin{cases} \bar{\varphi}^0 & \text{on } \Gamma_\varphi^\varepsilon, \\ 0 & \text{on } \Gamma_*^\varepsilon. \end{cases} \end{aligned} \quad (12)$$

Now the weak formulation for Case CFD\* can be established: given volume force  $\mathbf{f}^\varepsilon$  and charge  $q_E^\varepsilon$  and the functions involved in the boundary conditions (10), find  $(\mathbf{u}^\varepsilon, \varphi^\varepsilon, \bar{p}^\varepsilon) \in \mathbf{U}(\Omega_{m*}^\varepsilon) \times \mathcal{W}_*(\Omega_m^\varepsilon, \Gamma_\varphi^\varepsilon, \bar{\varphi}^0) \times \mathbb{R}$  such that:

$$\begin{aligned} \int_{\Omega_m^\varepsilon} [\mathbb{A}^\varepsilon \mathbf{e}(\mathbf{u}^\varepsilon) - (\underline{\mathbf{g}}^\varepsilon)^T \cdot \nabla \varphi^\varepsilon] : \mathbf{e}(\mathbf{v}) \, dV + \int_{\Omega_*^\varepsilon} [\mathbb{A}^\varepsilon \mathbf{e}(\mathbf{u}^\varepsilon)] : \mathbf{e}(\mathbf{v}) \, dV \\ - \bar{p}^\varepsilon \int_{\Gamma_c^\varepsilon} \mathbf{n}^{[c]} \cdot \mathbf{v} \, dS = \int_{\Gamma_\sigma^\varepsilon} \mathbf{h}^\varepsilon \cdot \mathbf{v} \, dS + \int_{\Omega_{m*}^\varepsilon} \mathbf{f}^\varepsilon \cdot \mathbf{v} \, dV, \\ \int_{\Omega_m^\varepsilon} [\underline{\mathbf{g}}^\varepsilon : \mathbf{e}(\mathbf{u}^\varepsilon) + \mathbf{d}^\varepsilon \cdot \nabla \varphi^\varepsilon] \cdot \nabla \psi \, dV = \int_{\Omega_m^\varepsilon} q_E^\varepsilon \psi \, dV + \int_{\Gamma_D^\varepsilon \cup \Gamma_c^\varepsilon} \varrho_E^\varepsilon \psi \, dS, \\ \int_{\partial\Omega_c^\varepsilon} \widetilde{\mathbf{u}}^\varepsilon \cdot \mathbf{n}^{[c]} \, dS + \gamma^\alpha \bar{p}^\varepsilon |\Omega_c^\varepsilon| = -J^\varepsilon, \end{aligned} \quad (13)$$

for all  $(\mathbf{v}, \psi) \in \mathbf{U}_0(\Omega_{m*}^\varepsilon) \times \mathcal{W}_0(\Omega_m^\varepsilon, \Gamma_\varphi^\varepsilon)$ . Note that by virtue of the set  $\mathcal{V}_*(\Omega_m^\varepsilon, \Gamma_*^\varepsilon)$  defined in (11), the solution  $\varphi^\varepsilon$  satisfies the constraint (9)<sub>5,6</sub>. We recall that the potential  $\bar{\varphi}^0$  is prescribed on a nonvanishing part of  $\Gamma_\varphi^\varepsilon$ , see (11), which is necessary to ensure a unique solution of (13). It is worth to note that, in (13)<sub>1</sub>, the normal  $\mathbf{n}^{[c]}$  is employed instead of normals outward w.r.t. the solid skeleton.

**Remark 2.2.** *In the above formulation,  $\bar{\varphi}^{k,\varepsilon}$  involved in the set  $\mathcal{V}_*(\Omega_m^\varepsilon, \Gamma_*^\varepsilon)$  are considered as unknown potentials associated with the conductor parts, whereby, in the sense of test functions, the corresponding test potential, say  $\bar{\psi}^{k,\varepsilon}$  can be associated arbitrary values. However, as a modification of the problem,  $\bar{\varphi}^{k,\varepsilon}$  could also be considered as given constants. Then the only difference in the formulation is that  $\varphi^\varepsilon \in \mathcal{V}_*(\Omega_m^\varepsilon, \Gamma_*^\varepsilon, \bar{\varphi})$  and correspondingly the set of the test potentials is replaced by  $\mathcal{V}_0(\Omega_m^\varepsilon, \Gamma_*^\varepsilon)$ ; recall that also  $\Gamma_\varphi^\varepsilon = \emptyset$  in this case.*

In this paper we shall focus on the two combination of the cases listed above, namely CFD\* and DFC\*. For both these types of microstructures we first restrict to the no flow situations, thus, considering uniform pressure in each connected domain filled with fluid.

### 3. Homogenization of the static problem – case CFD\*

In this section we are concerned with a steady state of the porous medium which is in the thermodynamic equilibrium characterized by static fluid in the channels and vanishing fluid pressure gradients.

The homogenization methods based on the two scale convergence or the unfolding operator techniques [5] can be applied to describe the limit models arising from asymptotic analyses of the problem (13) for  $\varepsilon \rightarrow 0$ . Although, in this paper, we skip presentation of some of the mathematical analysis which has been done to prove the convergence result, we explain the main steps in the derivation of the local problems for computing the so-called characteristic responses and the macroscopic model equations.

#### 3.1. Representative periodic cell and its decomposition

In accordance with the decomposition (1) of domain  $\Omega$ , the fluid saturated porous medium is generated by a reference periodic cell  $Y$  decomposed into three non-overlapping subdomains  $Y_m$ ,  $Y_c$  and  $Y_*$ , see Fig. 1,

$$\begin{aligned} Y &= Y_m \cup Y_c \cup Y_* \cup \Gamma_Y, \\ Y_i \cap Y_j &= \emptyset \text{ for } j \neq i \text{ with } i, j \in \{c, m, *\}, \\ Y_* &= \bigcup_k Y_*^k, \quad Y_*^k \cap Y_*^l = \emptyset \text{ for } k \neq l, \\ \text{dist}(Y_*^k, Y_*^l) &\geq s^*(1 - \delta_{kl}), \quad s^* > 0, \end{aligned} \tag{14}$$

where  $s^*$  is the minimum distance of the conductive parts and  $\Gamma_Y$ , representing the union of all the interfaces, splits in three disjoint parts (in the sense of the surface measure),

$$\begin{aligned} \Gamma_Y &= \Gamma_{mc} \cup \Gamma_{m*} \cup \Gamma_{c*}, \\ \Gamma_{mc} &= \overline{Y_m} \cap \overline{Y_c}, \\ \Gamma_{m*}^k &= \overline{Y_*^k} \cap \overline{Y_m} \quad \text{and} \quad \Gamma_{d*} = \overline{Y_d} \cap \overline{Y_*}, \quad d \in \{c, m\}. \end{aligned} \tag{15}$$

For the Case D\* we assume well separated conductor parts, *i.e.*  $\overline{Y_*^k} \cap \partial Y = \emptyset$ , such that the lattice generated by one (rescaled) conductor  $Z_*^{k,\varepsilon} = \varepsilon Y_*^k$  forms mutually disconnected inclusions with the perimeter  $\approx \varepsilon$ .

We shall need some further notation. By  $\mathbf{H}_\#^1(Y_m)$  we refer to the Sobolev space of vector-valued  $Y$ -periodic functions (indicated by the subscript  $\#$ ). By  $\mathcal{f}_D = |Y|^{-1} \int_D$  with  $D \subset \overline{Y}$  we denote the local average, although  $|Y| = 1$  can always be chosen. Further we need the space  $\widetilde{\mathbf{H}}_\#^1(Y_m)$  which is a restriction of  $\mathbf{H}_\#^1(Y_m)$  to functions with the vanishing average, thus, any  $\mathbf{w} \in \widetilde{\mathbf{H}}_\#^1(Y_m)$  satisfies  $\mathcal{f}_D \mathbf{w} = 0$ ; the space  $\widetilde{H}_\#^1(Y_m)$  is defined in analogy. We also employ  $\mathbf{\Pi}^{ij} = (\Pi_k^{ij})$ ,  $i, j, k = 1, 2, 3$  with components  $\Pi_k^{ij} = y_j \delta_{ik}$ .

The following space and sets will be employed in Sections 3 and 4:

$$\begin{aligned} H_{\#0*}^1(Y_m) &= \{\psi \in H_\#^1(Y_m) \mid \psi = 0 \text{ on } \Gamma_{m*}\}, \\ H_{\#0,k}^1(Y_m) &= \{\psi \in H_\#^1(Y_m) \mid \psi = \delta_{ki} \text{ on } \Gamma_{m*}^i, i = 1, 2, \dots, k^*\}, \\ W_{\#*}(Y_m) &= \{\psi \in \widetilde{H}_\#^1(Y_m) \mid \exists (a_k) : \psi = \sum_k a_k \hat{\varphi}^k, \forall \hat{\varphi}^k \in H_{\#0,k}^1(Y_m)\}. \end{aligned} \quad (16)$$

### 3.2. Asymptotic expansions

To use the unfolding method of homogenization, or the two-scale convergence method, a priori estimates on the solution to the problem (13) should be obtained. For this, it is necessary to scale appropriately the surface charge prescribed on the interfaces  $\Gamma_{cm}^\varepsilon$ , see (9)<sub>2</sub>. We assume constant interface charges  $\bar{\rho}_E$ , such that  $(\chi_{mc}(y))$  is the characteristic function of  $\Gamma_{mc}$

$$\mathcal{T}_\varepsilon(\varrho_E^\varepsilon(x)) = \varepsilon \bar{\rho}_E \chi_{mc}(y). \quad (17)$$

The a priori estimates can be derived using the Korn, Poincaré and Young inequalities upon substituting suitable test functions into (13), so that obvious manipulations yield the following uniform estimates:

$$\|\mathbf{u}^\varepsilon\|_{\mathbf{H}^1(\Omega_m^\varepsilon \cup \Omega_*^\varepsilon)} + \|\varphi^\varepsilon\|_{L^2(\Omega_m^\varepsilon)} + \|\nabla \varphi^\varepsilon\|_{L^2(\Omega_m^\varepsilon)} \leq C, \quad (18)$$

where the r.h.s. constant  $C$ , being independent of  $\varepsilon$ , depends on all the data inherited from the boundary conditions, volume forces and electric charges. As the consequence, the following weak convergences hold:

$$\begin{aligned} \mathcal{T}_\varepsilon(\mathbf{u}^\varepsilon) &\rightharpoonup \mathbf{u}^0 \quad \text{in } \mathbf{L}^2(\Omega \times Y_{m*}), \\ \mathcal{T}_\varepsilon(\nabla \mathbf{u}^\varepsilon) &\rightharpoonup \nabla_x \mathbf{u}^0 + \nabla_y \mathbf{u}^1 \quad \text{in } \mathbf{L}^2(\Omega \times Y_{m*}), \\ \mathcal{T}_\varepsilon(\varphi^\varepsilon) &\rightharpoonup \varphi^0 \quad \text{in } L^2(\Omega \times Y_m), \\ \mathcal{T}_\varepsilon(\nabla \varphi^\varepsilon) &\rightharpoonup \nabla_x \varphi^0 + \nabla_y \varphi^1 \quad \text{in } L^2(\Omega \times Y_m), \end{aligned} \quad (19)$$

where  $\mathbf{u}^1 \in L^2(\Omega; \mathbf{H}_{\#}^1(Y_{m*}))$ ,  $\varphi^1 \in L^2(\Omega; H_{\#}^1(Y_m))$  and  $\mathbf{u}^0 \in \mathbf{H}^1(\Omega)$ ,  $\varphi^0 \in H^1(\Omega)$ . We recall that  $\mathbf{u}^{1\varepsilon}$  and  $\varphi^{1\varepsilon}$  are  $Y$ -periodic in the second argument.

Due to the interface condition (9), it can be proved that

$$\varphi^1(x, \cdot) = \bar{\varphi}^k(x) \quad \text{on } \Gamma_*^k \text{ for any } x \in \Omega, \quad (20)$$

therefore  $\varphi^1 \in L(\Omega; W_{\#*}(Y_m))$ , see (16). Note that  $\bar{\varphi}^k$  is an unknown field which can be determined once  $\varphi^1(x, \cdot)$  is computed.

By virtue of the asymptotic expansion method, the solution of problem (13) can be established in the form of the following truncated expansions expressed in the unfolded forms

$$\begin{aligned} \mathcal{T}_\varepsilon(\mathbf{u}^\varepsilon) &\approx \mathbf{u}^{R\varepsilon}(x, y) := \mathbf{u}^{0\varepsilon}(x) + \varepsilon \mathbf{u}^{1\varepsilon}(x, y), \\ \mathcal{T}_\varepsilon(\varphi^\varepsilon) &\approx \varphi^{R\varepsilon}(x) := \varphi^{0\varepsilon}(x) + \varepsilon \varphi^{1\varepsilon}(x, y), \end{aligned} \quad (21)$$

where the local coordinates  $y$  are related to the global ones by the mapping  $y_k = \mathcal{Y}_k(x)$  defined in Section 2.1. As a consequence, the test functions  $\mathbf{v}^\varepsilon$  and  $\psi^\varepsilon$  associated with  $\mathbf{u}^\varepsilon$  and  $\varphi^\varepsilon$  are considered in the same form of the truncated expansions (21) constituted by  $\mathbf{v}^0, \mathbf{v}^1, \psi^0$ , and  $\psi^1$ .

### 3.3. Local problems

Due to the convergence result, the limit in the weak formulation (13) with test functions  $\mathcal{T}_\varepsilon(\mathbf{u}^\varepsilon(x)) = \varepsilon \mathbf{v}^1(x, y)$  and  $\mathcal{T}_\varepsilon(\psi^\varepsilon(x)) = \varepsilon \psi^1(x, y)$  yield the local equations,

$$\begin{aligned} &\int_{\Omega \times Y_*} \nabla_y^S \mathbf{v}^1 : \mathbb{A} (\nabla_x^S \mathbf{u}^0 + \nabla_y^S \mathbf{u}^1) \, dV_{xy} \\ &\quad + \int_{\Omega \times Y_m} \nabla_y^S \mathbf{v}^1 : [\mathbb{A} (\nabla_x^S \mathbf{u}^0 + \nabla_y^S \mathbf{u}^1) - \underline{\mathbf{g}}^T \cdot (\nabla_x \varphi^0 + \nabla_y \varphi^1)] \, dV_{xy} \\ &\quad = \bar{p} \int_{\Omega} \int_{\Gamma_c} \mathbf{v}^1 \cdot \mathbf{n}^{[c]} \, dS_y \, dV_x, \\ &\int_{\Omega \times Y_m} \nabla_y \psi^1 \cdot [\underline{\mathbf{g}} : (\nabla_x^S \mathbf{u}^0 + \nabla_y^S \mathbf{u}^1) + \mathbf{d}(\nabla_x \varphi^0 + \nabla_y \varphi^1)] \, dV_{xy} = 0, \end{aligned} \quad (22)$$

for all  $\mathbf{v}^1 \in \mathbf{L}^2(\Omega; \mathbf{H}_{\#}^1(Y_m))$  and  $\psi^1 \in L^2(\Omega; W_{\#*}(Y_m))$ . Note that by symbols  $dV$ ,  $dV_{xy}$ ,  $dV_x$ ,  $dV_y$ ,  $dS$ ,  $dS_x$  and  $dS_y$  we refer to the elementary volumes and surfaces w.r.t. the different spatial scales.

Due to the linearity of this problem, the fluctuations  $\mathbf{u}^1$  and  $\varphi^1$  can be expressed in terms of the macroscopic variables:

$$\begin{aligned}\mathbf{u}^1(x, y) &= \boldsymbol{\omega}^{ij} e_{ij}^x(\mathbf{u}^0) + \boldsymbol{\omega}^k \partial_k^x \varphi^0 - \bar{p} \boldsymbol{\omega}^P, \\ \varphi^1(x, y) &= \eta^{ij} e_{ij}^x(\mathbf{u}^0) + \eta^k \partial_k^x \varphi^0 - \bar{p} \eta^P,\end{aligned}\quad (23)$$

where  $\boldsymbol{\omega} \in \mathbf{H}_{\#}^1(Y_m)$  and  $\eta \in H_{\#}^1(Y_m)$  are characteristic responses of displacements and electric potential in the matrix part  $Y_m$ .

If the structure is perfectly periodic, the decomposition of the microstructure and the microstructure parameters are independent of the macroscopic position  $x \in \Omega$ . Otherwise the local problems must be considered at any macroscopic position, i.e. for almost any  $x \in \Omega$ , cf. [24].

We shall use the following bilinear forms:

$$\begin{aligned}a_Y^{m*}(\mathbf{u}, \mathbf{v}) &= \int_{Y_m \cup Y_*} [\mathbb{A} \mathbf{e}_y(\mathbf{u})] : \mathbf{e}_y(\mathbf{v}) \, dV_y, \\ g_Y^m(\mathbf{u}, \psi) &= \int_{Y_m} g_{kij} e_{ij}^y(\mathbf{u}) \partial_k^y \psi \, dV_y, \\ d_Y^m(\varphi, \psi) &= \int_{Y_m} [\mathbf{d} \nabla_y \varphi] \cdot \nabla_y \psi \, dV_y.\end{aligned}\quad (24)$$

The local microstructural response is obtained by solving the following decoupled problems:

- Find  $(\boldsymbol{\omega}^{ij}, \eta^{ij}) \in \widetilde{\mathbf{H}}_{\#}^1(Y_m) \times W_{\#*}(Y_m)$  for any  $i, j = 1, 2, 3$  satisfying

$$\begin{aligned}a_Y^{m*}(\boldsymbol{\omega}^{ij} + \boldsymbol{\Pi}^{ij}, \mathbf{v}) - g_Y^m(\mathbf{v}, \eta^{ij}) &= 0, \quad \forall \mathbf{v} \in \mathbf{H}_{\#}^1(Y_m), \\ g_Y^m(\boldsymbol{\omega}^{ij} + \boldsymbol{\Pi}^{ij}, \psi) + d_Y^m(\eta^{ij}, \psi) &= 0, \quad \forall \psi \in W_{\#*}(Y_m),\end{aligned}\quad (25)$$

- Find  $(\boldsymbol{\omega}^k, \eta^k) \in \widetilde{\mathbf{H}}_{\#}^1(Y_m) \times W_{\#*}(Y_m)$  for any  $k = 1, 2, 3$  satisfying

$$\begin{aligned}a_Y^{m*}(\boldsymbol{\omega}^k, \mathbf{v}) - g_Y^m(\mathbf{v}, \eta^k + y_k) &= 0, \quad \forall \mathbf{v} \in \mathbf{H}_{\#}^1(Y_m), \\ g_Y^m(\boldsymbol{\omega}^k, \psi) + d_Y^m(\eta^k + y_k, \psi) &= 0, \quad \forall \psi \in W_{\#*}(Y_m),\end{aligned}\quad (26)$$

- Find  $(\boldsymbol{\omega}^P, \eta^P) \in \widetilde{\mathbf{H}}_{\#}^1(Y_m) \times W_{\#*}(Y_m)$  satisfying

$$\begin{aligned}a_Y^{m*}(\boldsymbol{\omega}^P, \mathbf{v}) - g_Y^m(\mathbf{v}, \eta^P) &= - \int_{\Gamma_c} \mathbf{v} \cdot \mathbf{n}^{[c]} \, dS_y, \quad \forall \mathbf{v} \in \mathbf{H}_{\#}^1(Y_m), \\ g_Y^m(\boldsymbol{\omega}^P, \psi) + d_Y^m(\eta^P, \psi) &= 0, \quad \forall \psi \in W_{\#*}(Y_m),\end{aligned}\quad (27)$$

### 3.4. Macroscopic model

Using the local corrector basis functions we are able to introduce the homogenized coefficients which describe the effective poroelastic properties at the mesoscopic scale. Since the porosity is open on  $\partial\Omega$  we need to assume convergence of the boundary segments  $\Gamma_\sigma^\varepsilon, \Gamma_{\bar{D}}^\varepsilon, \Gamma_{\mathbf{u}}^\varepsilon$  and  $\Gamma_\varphi^\varepsilon$  to  $\partial_\sigma\Omega, \partial_{\bar{D}}\Omega, \partial_{\mathbf{u}}\Omega$  and  $\partial_\varphi\Omega$ . In the limit, the boundary conditions (10) respected by the sets (11) induce the following admissibility sets:  $\mathbf{U}(\Omega) = \{\mathbf{v} \in \mathbf{H}^1(\Omega) \mid \mathbf{v} = \bar{\mathbf{u}} \text{ on } \partial_{\mathbf{u}}\Omega\}$  and  $\mathcal{V}(\Omega) = \{\psi \in H^1(\Omega) \mid \psi = \bar{\varphi}^0 \text{ on } \partial_\varphi\Omega\}$ . The associated spaces of test functions are  $\mathbf{U}_0(\Omega)$  and  $\mathcal{V}_0(\Omega)$ . The test displacements belong to space  $\mathbf{U}_0(\Omega)$  which is restriction of  $\mathbf{U}(\Omega)$  to functions vanishing on  $\partial_{\mathbf{u}}\Omega$ . In analogy, the test potentials belong to space  $\mathcal{V}_0(\Omega)$  which is defined by virtue of  $\mathcal{V}(\Omega)$  by all functions from  $H^1(\Omega)$  vanishing on  $\partial_\varphi\Omega$ .

The limit global problem is obtained from (13) with test functions  $\mathcal{T}_\varepsilon(\mathbf{u}^\varepsilon(x)) = \varepsilon \mathbf{v}^0(x)$  and  $\mathcal{T}_\varepsilon(\psi^\varepsilon(x)) = \varepsilon \psi^0(x)$ . The couple  $(\mathbf{u}^0, \varphi^0) \in \mathbf{U}(\Omega) \times H^1(\Omega)/\mathbb{R}$  and  $\bar{p} \in \mathbb{R}$  satisfies

$$\begin{aligned}
& \int_{\Omega} e_{ij}^x(\mathbf{v}^0) [a_Y^{m*}(\mathbf{u}^1 - \mathbf{\Pi}^{kl} e_{kl}^x(\mathbf{u}^0), \mathbf{\Pi}^{ij}) - g_Y^m(\mathbf{\Pi}^{ij}, \varphi^1 + y_k \partial_k^x \phi^0)] \, dV_x \\
& - \bar{p} \int_{\Omega} \phi \nabla_x \cdot \mathbf{v}^0 \, dV_x = \int_{\Omega} \hat{\mathbf{f}} \cdot \mathbf{v}^0 \, dV_x + \int_{\partial\Omega} \bar{\mathbf{h}}(\bar{p}) \cdot \mathbf{v}^0 \, dS_x, \\
& \int_{\Omega} \partial_i^x \psi^0 [g_Y^m(\mathbf{u}^1 - \mathbf{\Pi}^{kl} e_{kl}^x(\mathbf{u}^0), y_i) + d_Y^m(\varphi^1 + y_k \partial_k^x \phi^0, y_i)] \, dV_x \quad (28) \\
& = \int_{\Omega} \hat{q}_E \psi^0 \, dV_x + \int_{\partial\Omega} \bar{q}_E \psi^0 \, dS_x, \\
& \int_{\Omega} \left( \phi \nabla_x \cdot \mathbf{u} - \int_{\Gamma_Y} \mathbf{u}^1 \cdot \mathbf{n}^{[m]} \, dS_y \right) \, dV_x + \bar{p} \gamma \phi |\Omega| = -J,
\end{aligned}$$

for all  $(\mathbf{v}^0, \psi^0) \in \mathbf{U}_0(\Omega) \times H^1(\Omega)$ , where  $(\mathbf{u}^1, \varphi^1)$  depends on  $(\mathbf{u}^0, \varphi^0)$  by virtue of the local problem (22). Above the volume charge is  $\hat{\rho}_E := \tilde{\rho}_E + |\Gamma_{cm}|/|Y| \bar{\rho}_E$ , where  $\tilde{\rho}_E = \int_{Y_m} \mathcal{T}_\varepsilon(\rho_E^\varepsilon)$ . Thus, the constant surface charges defined in (17) constitute the effective volume charges involved in the macroscopic model. Further,  $\bar{q}_E = \bar{\phi}_m \rho_E$  is the effective surface charge.

The volume forces  $\hat{\mathbf{f}}$  and boundary tractions  $\bar{\mathbf{h}}(\bar{p})$  are derived in analogy with the treatment explained in [21], thus,  $\hat{\mathbf{f}} = \phi_{m*} \mathbf{f}$  and  $\bar{\mathbf{h}}(\bar{p}) = \bar{\phi}_{m*} \mathbf{h} - \mathbf{n}(1 - \bar{\phi}_{m*}) \bar{p}$ , where  $\phi_{m*}$  and  $\bar{\phi}_{m*}$  are the volume and surface fractions of the solid phase; while  $\phi_{m*} = |Y_{m*}|/|Y|$ , the surface fraction is defined ad hoc, depending on given assumptions about porosity of the external surface  $\partial\Omega$ . Obviously, the imposed boundary conditions must be coherent with these



assumptions. It is worth noting that here  $\bar{\mathbf{h}}(\bar{p})$  applies as the limit surface force to the situation of the static loading with the drained conditions on the external pore boundary  $\partial_{\text{ext}}\Omega_c^\varepsilon$ . Obviously, for the case DF, when only fluid inclusions are considered, the surface porosity is zero, thus,  $\bar{\phi}_{m^*} = 1$ .

The characteristic responses (25)–(27) obtained at the microscopic scale allow us to express the local averaging integrals in (28) involving the two-scale functions using the homogenized coefficients. Their expressions are identified upon substituting the split (23) into the three equations in (28): In the equilibrium equation:

$$\begin{aligned} A_{klij}^H &= a_Y^{m^*} (\boldsymbol{\omega}^{ij} + \boldsymbol{\Pi}^{ij}, \boldsymbol{\Pi}^{kl}) - g_Y^m (\boldsymbol{\Pi}^{kl}, \eta^{ij}) \\ &= a_Y^{m^*} (\boldsymbol{\omega}^{ij} + \boldsymbol{\Pi}^{ij}, \boldsymbol{\omega}^{kl} + \boldsymbol{\Pi}^{kl}) + d_Y^m (\eta^{kl}, \eta^{ij}) , \\ B_{ij}^H &= a_Y^{m^*} (\boldsymbol{\omega}^P, \boldsymbol{\Pi}^{ij}) - g_Y^m (\boldsymbol{\Pi}^{ij}, \eta^P) + \phi \delta_{ij} , \\ G_{kij}^H &= g_Y^m (\boldsymbol{\Pi}^{ij}, \eta^k + y_k) - a_Y^{m^*} (\boldsymbol{\omega}^k, \boldsymbol{\Pi}^{ij}) . \end{aligned} \quad (29)$$

In the electricity equation:

$$\begin{aligned} \acute{G}_{kij}^H &= g_Y^m (\boldsymbol{\omega}^{kl} + \boldsymbol{\Pi}^{kl}, y_k) + d_Y^m (\eta^{ij}, y_k) , \\ D_{kl}^H &= g_Y^m (\boldsymbol{\omega}^l, y_k) + d_Y^m (\eta^l + y_l, y_k) \\ &= d_Y^m (\eta^l + y_l, \eta^k + y_k) + a_Y^{m^*} (\boldsymbol{\omega}^k, \boldsymbol{\omega}^l) , \\ \acute{F}_i^H &= g_Y^m (\boldsymbol{\omega}^P, y_i) + d_Y^m (\eta^P, y_i) . \end{aligned} \quad (30)$$

In the fluid mass conservation equation:

$$\begin{aligned} \acute{B}_{ij}^H &= - \int_{Y_m} \text{div}_y \boldsymbol{\omega}^{ij} dV_y + \phi \delta_{ij} = a_Y^{m^*} (\boldsymbol{\omega}^P, \boldsymbol{\Pi}^{ij}) - g_Y^m (\boldsymbol{\Pi}^{ij}, \eta^P) + \phi \delta_{ij} , \\ M^H &= \int_{\Gamma_Y} \boldsymbol{\omega}^P \cdot \mathbf{n}^{[m^*]} dS_y + \gamma \phi = a_Y^{m^*} (\boldsymbol{\omega}^P, \boldsymbol{\omega}^P) + d_Y^m (\eta^P, \eta^P) + \gamma \phi , \\ F_i^H &= \int_{\Gamma_Y} \boldsymbol{\omega}^i \cdot \mathbf{n}^{[m^*]} dS_y . \end{aligned} \quad (31)$$

It is worth noting that the effective elasticity  $\mathbb{A}^H = (A_{klij}^H)$  inherits all the symmetry properties of the piezoelectric material elasticity  $\mathbb{D}$ . Also the other poroelastic coefficients, namely the symmetric Biot stress-coupling coefficient  $B_{ij}^H$ , and the positive Biot compressibility coefficient  $M^H$ , reflect the piezoelectric properties of the skeleton. The expressions proving the symmetry and positivity properties are obtained using (25)–(27).

Now we can rewrite equations (28) of the global problem in terms of the homogenized coefficients (29)-(31),

$$\begin{aligned}
\int_{\Omega} [\mathbb{A}^H \mathbf{e}(\mathbf{u}^0) - (\underline{\mathbf{G}}^H)^T \nabla \varphi^0 - \bar{p} \mathbf{B}^H] : \mathbf{e}(\mathbf{v}^0) \, dV_x &= \int_{\Omega} \hat{\mathbf{f}} \cdot \mathbf{v}^0 \, dV_x + \int_{\partial\Omega} \bar{\mathbf{h}}(\bar{p}) \cdot \mathbf{v}^0 \, dS_x, \\
\int_{\Omega} [\underline{\mathbf{G}}^H \mathbf{e}(\mathbf{u}^0) + \mathbf{D}^H \nabla \varphi^0 - \hat{\mathbf{F}}^H \bar{p}] \cdot \nabla \psi^0 \, dV_x &= \int_{\Omega} \hat{q}_E \psi^0 \, dV_x + \int_{\partial\Omega} \overline{\partial E} \psi^0 \, dS_x, \\
\int_{\Omega} (\hat{\mathbf{B}}^H : \mathbf{e}(\mathbf{u}^0) - \mathbf{F}^H \cdot \nabla \varphi^0 + M^H \bar{p}) \, dV_x &+ \bar{p} \gamma |\Omega| = -J.
\end{aligned} \tag{32}$$

In accordance with phenomenological theory, one should expect the Onsager reciprocity relationships to be satisfied, which is one of the advantageous features of the homogenization method. Indeed, the following equalities are proved in the Appendix A,

$$F_i^H = \hat{F}_i^H, \quad G_{kij}^H = \hat{G}_{kij}^H, \quad B_{ij}^H = \hat{B}_{ij}^H. \tag{33}$$

Using the symmetry relationships (33), the macroscopic problem (32) can be reformulated, as follows: Find  $(\mathbf{u}^0, \varphi^0) \in \mathbf{U}(\Omega) \times \mathcal{V}(\Omega)$  and  $\bar{p} \in \mathbb{R}$ , such that

$$\begin{aligned}
\int_{\Omega} [\mathbb{A}^H \mathbf{e}(\mathbf{u}^0) - (\underline{\mathbf{G}}^H)^T \nabla \varphi^0 - \bar{p} \mathbf{B}^H] : \mathbf{e}(\mathbf{v}^0) \, dV_x &= \int_{\Omega} \hat{\mathbf{f}} \cdot \mathbf{v}^0 \, dV_x + \int_{\partial_{\sigma}\Omega} \bar{\mathbf{h}}(\bar{p}) \cdot \mathbf{v}^0 \, dS_x, \\
\int_{\Omega} [\underline{\mathbf{G}}^H \mathbf{e}(\mathbf{u}^0) + \mathbf{D}^H \nabla \varphi^0 - \mathbf{F}^H \bar{p}] \cdot \nabla \psi^0 \, dV_x &= \int_{\Omega} \hat{q}_E \psi^0 \, dV_x + \int_{\partial_D\Omega} \overline{\partial E} \psi^0 \, dS_x, \\
\int_{\Omega} (\mathbf{B}^H : \mathbf{e}(\mathbf{u}^0) - \mathbf{F}^H \cdot \nabla \varphi^0 + M^H \bar{p}) \, dV_x &= -J,
\end{aligned} \tag{34}$$

for all  $(\mathbf{v}^0, \psi^0) \in \mathbf{U}_0(\Omega) \times \mathcal{V}_0(\Omega)$ .

From (34), the strong form of the macroscopic problem can be obtained. We present a generalized formulation which admits both the cases CF and DF, the latter deduced for the separated inclusions, thus, giving rise the locally defined fluid pressure  $p(x)$ ; we are concerned with this case in the next section. The equilibrium equations and the boundary conditions( we

drop the superscripts <sup>0</sup>),

$$\begin{aligned}
-\nabla \cdot \boldsymbol{\sigma}^H(\mathbf{u}, \varphi, p) &= \hat{\mathbf{f}}, & \text{in } \Omega, \\
\nabla \cdot \vec{D}^H(\mathbf{u}, \varphi, p) &= \hat{q}_E, & \text{in } \Omega, \\
\boldsymbol{\sigma}^H(\mathbf{u}, \varphi, p) \cdot \mathbf{n} &= \bar{\mathbf{h}}, & \text{on } \partial_\sigma \Omega, \\
\vec{D}^H(\mathbf{u}, \varphi, p) \cdot \mathbf{n} &= -\bar{\varrho}_E, & \text{on } \partial_D \Omega
\end{aligned} \tag{35}$$

involve the effective constitutive equations for the upscaled porous piezoelectric material:

$$\begin{aligned}
\boldsymbol{\sigma}^H &= \mathbb{A}^H \mathbf{e}(\mathbf{u}) - (\underline{\mathbf{G}}^H)^T \nabla \varphi - p \mathbf{B}^H, \\
\vec{D} &= \underline{\mathbf{G}}^H \mathbf{e}(\mathbf{u}) + \mathbf{D}^H \nabla \varphi - \mathbf{F}^H p, \\
-p &= \frac{1}{M^H} (\mathbf{B}^H : \mathbf{e}(\mathbf{u}) - \mathbf{F}^H \cdot \nabla \varphi + j),
\end{aligned} \tag{36}$$

where  $p = \bar{p}$  and  $j = J/|\Omega|$  is the local fluid volume production in the porous material per volume.

**Remark 3.1.** *Although, in this study, we consider static loading such that no pressure gradients appear, the homogenization result can be extended for quasistatic, nonstationary problems. To do so, we consider  $p$  as a scalar field depending on  $x$ , and put  $j = \nabla \cdot \mathbf{w}$ , where  $\mathbf{w}$  is the seepage velocity, cf. [22], where an analogous treatment was pursued.*

As the consequence of (36), the pressure can be eliminated from the (36)<sub>1,2</sub>, so that

$$\begin{aligned}
\boldsymbol{\sigma}^H &= \mathbb{A}^U \mathbf{e}(\mathbf{u}) - (\underline{\mathbf{G}}^U)^T \nabla \varphi + (M^H)^{-1} \mathbf{B}^H j, \\
\vec{D} &= \underline{\mathbf{G}}^U \mathbf{e}(\mathbf{u}) + \mathbf{D}^U \nabla \varphi + (M^H)^{-1} \mathbf{F}^H j,
\end{aligned} \tag{37}$$

where the following coefficients labelled by superscript <sup>U</sup> can be considered as the “undrained” effective material properties:

$$\begin{aligned}
\mathbb{A}^U &= \mathbb{A}^H + (M^H)^{-1} \mathbf{B}^H \otimes \mathbf{B}^H && \text{undrained elasticity,} \\
\mathbf{D}^U &= \mathbf{D}^H - (M^H)^{-1} \mathbf{F}^H \otimes \mathbf{F}^H && \text{undrained dielectricity,} \\
\underline{\mathbf{G}}^U &= \underline{\mathbf{G}}^H + (M^H)^{-1} \mathbf{F}^H \mathbf{B}^H && \text{undrained piezoelectric coupling.}
\end{aligned} \tag{38}$$

It should be noticed that for  $J = 0$ , *i.e.* in the undrained situation, (37) gives the constitutive law which is analogous to a piezoelectric solid. The final

remark concerns the electric field generated alternatively by pore pressure, or by the fluid injection. If the macroscopic strains vanish  $\mathbf{e}(\mathbf{u}) = 0$ , then

$$\nabla\varphi = (\mathbf{D}^H)^{-1}\mathbf{F}^H\bar{p}, \quad \text{or} \quad \nabla\varphi = -(\hat{M}\mathbf{D}^U)^{-1}\mathbf{F}^Hj.$$

#### 4. Homogenization of the static problem – case DFC\*

In this section we treat the problem with prescribed voltage on a finite number of mutually disconnected conductor networks penetrating into the period structure of the porous material. As a consequence, if the electric field is getting stronger with  $\varepsilon \rightarrow 0$ , also the dielectric properties of the piezoelectric material must be decreasing in the right order, so that the electric displacements remain bounded.

##### 4.1. Microstructures and material scaling

We consider formulation (13) with given potentials  $\bar{\varphi}^k$  for each simply connected domain  $\Omega_*^{k,\varepsilon}$  occupied by the perfect conductor and represented by  $Y_*^k$  within the cell  $Y$ . We shall assume that on the external boundary of the piezoelectric structure no voltage is prescribed, thus,  $\Gamma_\varphi^\varepsilon = \emptyset$ , see (3) and (10). The following two cases can be considered:

(W) Weakly controlled field:  $\bar{\varphi}^{k,\varepsilon} = \varepsilon\bar{\varphi}^k$ ;

(S) Strongly controlled field:  $\bar{\varphi}^{k,\varepsilon} = \bar{\varphi}^k$ .

In both these cases,  $\bar{\varphi}^k$  is independent of  $\varepsilon$ . It can be shown that the convergence result related to the potential  $\varphi^\varepsilon$  of the model treated above in Section 3 can be adapted easily for the case DFC\*W, which leads to the same limit homogenized mode, as the one introduced before. Therefore, here we focus on the media with strongly controlled potentials, namely on the case DFC\*S.

Since  $\bar{\varphi}^k$  does not vanish with  $\varepsilon \rightarrow 0$ , steep gradients on the electric potential are assumed for small  $\varepsilon$ . As the consequence, to preserve finite electric field in the limit, we consider the following scaling of the dielectric and piezoelectric coefficients:

$$\left. \begin{aligned} \underline{\mathbf{g}}^\varepsilon(x) &= \varepsilon\underline{\mathbf{g}}, \\ \underline{\mathbf{d}}^\varepsilon(x) &= \varepsilon^2\underline{\mathbf{d}}, \end{aligned} \right\} \quad \text{in } \Omega_m^\varepsilon. \quad (39)$$

Since we consider Case DF, *i.e.*  $\Omega_c^\varepsilon$  is represented by all inclusions  $\Omega_c^{j,\varepsilon}$ , in the no-flow condition, the pressure is distributed as a piecewise constant function attaining a constant value in any  $\Omega_c^{j,\varepsilon}$ . Therefore, we define the space  $\mathcal{P}(\Omega_c^\varepsilon) = \{p \in L^2(\Omega_c^\varepsilon) \mid p = \bar{p}^j \text{ in } \Omega_c^{j,\varepsilon}\}$  with  $\bar{p}^j \in \mathbb{R}$  is representing any constant. Obviously, the number of inclusions increases with  $\varepsilon^{-3}$ . As the consequence of the DF type porosity, we assume no pore intersects boundary  $\partial\Omega$  so that neither  $\Gamma_\sigma$ , nor  $\mathbf{h}^\varepsilon$  depend on  $\varepsilon$  in the boundary condition specified in (10).

Given the potential values  $\bar{\varphi}^0 = \{\bar{\varphi}^k\}$ ,  $k = 1, 2, \dots, k^*$  in each subdomain  $\Omega_*^{k,\varepsilon}$  of  $\Omega_*^\varepsilon$ , volume force  $\mathbf{f}^\varepsilon$ , volume charge  $q_E^\varepsilon$ , and the functions involved in the r.h.s. of (10), find  $(\mathbf{u}^\varepsilon, \varphi^\varepsilon, p^\varepsilon) \in \mathcal{U}(\Omega_m^\varepsilon) \times \mathcal{V}_*(\Omega_m^\varepsilon, \Gamma_*^\varepsilon, \bar{\varphi}) \times \mathcal{P}(\Omega_c^\varepsilon)$  such that:

$$\begin{aligned}
& \int_{\Omega_m^\varepsilon} [\mathbb{A}^\varepsilon \mathbf{e}(\mathbf{u}^\varepsilon) - \varepsilon(\bar{\mathbf{g}})^T \cdot \nabla \varphi^\varepsilon] : \mathbf{e}(\mathbf{v}) \, dV + \int_{\Omega_*^\varepsilon} [\mathbb{A}^\varepsilon \mathbf{e}(\mathbf{u}^\varepsilon)] : \mathbf{e}(\mathbf{v}) \, dV \\
& - \int_{\Gamma_\varepsilon^\varepsilon} p^\varepsilon \mathbf{n}^{[c]} \cdot \mathbf{v} \, dS = \int_{\Gamma_\sigma} \mathbf{h} \cdot \mathbf{v} \, dS + \int_{\Omega_{m*}^\varepsilon} \mathbf{f}^\varepsilon \cdot \mathbf{v} \, dV , \\
& \int_{\Omega_m^\varepsilon} [\varepsilon \bar{\mathbf{g}} : \mathbf{e}(\mathbf{u}^\varepsilon) + \varepsilon^2 \bar{\mathbf{d}} \cdot \nabla \varphi^\varepsilon] \cdot \nabla \psi \, dV = \int_{\Omega_m^\varepsilon} q_E^\varepsilon \psi \, dV + \int_{\Gamma_D^\varepsilon \cup \Gamma_\varepsilon^\varepsilon} \varrho_E^\varepsilon \psi \, dS , \\
& \int_{\partial\Omega_\varepsilon^\varepsilon} q \widetilde{\mathbf{u}}^\varepsilon \cdot \mathbf{n}^{[c]} \, dS + \gamma^\alpha \int_{\Omega_\varepsilon^\varepsilon} p^\varepsilon q \, dV = 0 ,
\end{aligned} \tag{40}$$

for all  $(\mathbf{v}, \psi, q) \in \mathcal{U}_0(\Omega_m^\varepsilon) \times \mathcal{V}_0(\Omega_m^\varepsilon, \Gamma_*^\varepsilon) \times \mathcal{P}(\Omega_c^\varepsilon)$ .

#### 4.2. Asymptotic expansions

We proceed in analogy with derivation of the CFD\* model reported in Section 3. First we obtain the a priori estimates. Recalling the scaling ansatz (17) for the surface charge and the scaling (39) concerning piezoelectric material coefficients, standard manipulations in (40) yield

$$\|\mathbf{u}^\varepsilon\|_{\mathbf{H}^1(\Omega_m^\varepsilon \cup \Omega_*^\varepsilon)} + \|\varphi^\varepsilon\|_{L^2(\Omega_m^\varepsilon)} + \varepsilon \|\nabla \varphi^\varepsilon\|_{L^2(\Omega_m^\varepsilon)} + \|p^\varepsilon\|_{L^2(\Omega_c^\varepsilon)} \leq C , \tag{41}$$

where the constant  $C$ , being independent of  $\varepsilon$ , reflects the data of the problem.

To respect the boundary conditions, recalling  $\bar{\varphi}^k$  are given constants for  $k = 1, \dots, k^*$ , we require

$$\varphi^\varepsilon = \bar{\varphi}^k \quad \text{on } \Omega \times \Gamma_{m*}^k , \tag{42}$$

where  $\Gamma_{m^*}^k$  is defined in (15).

Due to (41), the following convergences hold

$$\begin{aligned}
\mathcal{T}_\varepsilon(\mathbf{u}^\varepsilon) &\rightharpoonup \mathbf{u}^0 && \text{in } \mathbf{L}^2(\Omega \times Y_{m^*}) , \\
\mathcal{T}_\varepsilon(\nabla \mathbf{u}^\varepsilon) &\rightharpoonup \nabla_x \mathbf{u}^0 + \nabla_y \mathbf{u}^1 && \text{in } \mathbf{L}^2(\Omega \times Y_{m^*}) , \\
\mathcal{T}_\varepsilon(\varphi^\varepsilon) &\rightharpoonup \hat{\varphi}^0 && \text{in } L^2(\Omega \times Y_m) , \\
\varepsilon \mathcal{T}_\varepsilon(\nabla \varphi^\varepsilon) &\rightharpoonup \nabla_y \hat{\varphi}^0 && \text{in } L^2(\Omega \times Y_m) , \\
\mathcal{T}_\varepsilon(p^\varepsilon) &\rightharpoonup p^0 && \text{in } L^2(\Omega \times Y_c) .
\end{aligned} \tag{43}$$

Moreover, due to the trace theorem, the electric two-scale potential satisfies the conditions

$$\hat{\varphi}^0(x, \cdot) = \bar{\varphi}^k(x) \quad \text{on } \Gamma_*^k \text{ for any } x \in \Omega , \tag{44}$$

where  $\bar{\varphi}^k$  are given,  $k = 1, 2, \dots, k^*$ . This makes the difference with treatment in Section 3, see (20), dealing with the case CFD\*, there by  $\bar{\varphi}^k(x)$  we mean an unknown value of the potential attained on the interface  $\Gamma_*^k$ , thus,  $\bar{\varphi}^k$  is a part of the homogenized problem solution, contrary to the present situation.

We shall employ the space  $H_{\#0^*}^1(Y_m)$  and the set  $H_{\#0,k}^1(Y_m)$  introduced in (16). Now (43) and (44) yield  $\hat{\varphi}^0(x, \cdot) \in V_{\bar{\varphi}}(Y_m) := H_{\#0^*}^1(Y_m) + \sum_k \lambda_*^k \hat{\varphi}^k(x, \cdot) \bar{\varphi}^k(x)$  for any  $x \in \Omega$  with  $\hat{\varphi}^k(x, \cdot) \in H_{\#0,k}^1(Y_m)$ .

The convergence result enables to introduce formally the following truncated expansions of displacements and potential such that the limit equations can be derived:

$$\begin{aligned}
\mathcal{T}_\varepsilon(\mathbf{u}^\varepsilon) &\approx \mathbf{u}^{R\varepsilon}(x, y) := \mathbf{u}^{0\varepsilon}(x) + \varepsilon \mathbf{u}^{1\varepsilon}(x, y) , \\
\mathcal{T}_\varepsilon(\varphi^\varepsilon) &\approx \varphi^{R\varepsilon}(x, y) := \hat{\varphi}^{0\varepsilon}(x, y) , \\
\mathcal{T}_\varepsilon(p^\varepsilon) &\approx p^{R\varepsilon}(x, y) := p^{0\varepsilon}(x) .
\end{aligned} \tag{45}$$

where  $\mathbf{u}^{1\varepsilon}$  and  $\Phi^{0\varepsilon}$  are  $Y$ -periodic in the second argument. By virtue of (43), we assume the convergence of  $\mathbf{u}^{0,\varepsilon}$ ,  $\mathbf{u}^{1\varepsilon}$ ,  $\Phi^{0\varepsilon}$  and  $p^{0\varepsilon}$  to the limit functions  $\mathbf{u}^0$ ,  $\mathbf{u}^1$ ,  $\hat{\varphi}^0$  and  $p^0$ , respectively. In analogy with (45), the test functions  $\mathbf{v}^\varepsilon$ ,  $\hat{\psi}^\varepsilon$  and  $q$  are expressed in terms of  $\mathbf{v}^0$ ,  $\mathbf{v}^1$ ,  $\hat{\psi}^0$  and  $q^0$  which are associated with  $\mathbf{u}^{0\varepsilon}$ ,  $\mathbf{u}^{1,\varepsilon}$ ,  $\varphi^{0\varepsilon}$  and  $p^\varepsilon$ , respectively.

### 4.3. Local problems

We recall the notation of the fluid-solid interface:  $\Gamma_c = \Gamma_{mc} \cup \Gamma_{c^*}$  with the fluid-outward normal  $\mathbf{n}^{[c]}$ . Straightforward calculations lead to

$$\begin{aligned} & \int_{\Omega \times (Y_m \cup Y_*)} \mathbf{e}_y(\mathbf{v}^1) : \mathbb{A} (\nabla_x^S \mathbf{u}^0 + \nabla_y^S \mathbf{u}^1) \, dV_{xy} - \int_{\Omega \times Y_m} \mathbf{e}_y(\mathbf{v}^1) : \underline{\bar{\mathbf{g}}}^T \nabla_y \hat{\varphi}^0 \, dV_{xy} \\ &= \int_{\Omega} p^0 \int_{\Gamma_c} \mathbf{v}^1 \cdot \mathbf{n}^{[c]} \, dS_y \, dV_x, \\ & \int_{\Omega \times Y_m} \nabla_y \hat{\psi} \cdot [\underline{\bar{\mathbf{g}}} : (\nabla_x^S \mathbf{u}^0 + \nabla_y^S \mathbf{u}^1) + \bar{\mathbf{d}} \nabla_y \hat{\varphi}^0] \, dV_{xy} = \int_{\Omega \times \Gamma_{mc}} \bar{\rho}_E \hat{\psi} \, dV_{xy}, \end{aligned} \quad (46)$$

which holds for all  $\mathbf{v}^1 \in \mathbf{L}^2(\Omega; \mathbf{H}_{\#}^1(Y_m))$  and  $\hat{\psi} \in L^2(\Omega; W_{\#*}(Y_m))$ .

The two-scale functions can be expressed in terms of the characteristic responses  $(\boldsymbol{\omega}, \eta)$ , such that

$$\begin{aligned} \boldsymbol{\omega}^1(x, y) &= \boldsymbol{\omega}^{ij} e_{ij}^x(\mathbf{u}^0) - p^0 \boldsymbol{\omega}^P + \boldsymbol{\omega}^\rho \rho_E + \sum_k \hat{\boldsymbol{\omega}}^k \bar{\varphi}^k, \\ \varphi^0(x, y) &= \hat{\eta}^{ij} e_{ij}^x(\mathbf{u}^0) - p^0 \hat{\eta}^P + \hat{\eta}^\rho \rho_E + \sum_k \hat{\varphi}^k \bar{\varphi}^k. \end{aligned} \quad (47)$$

All  $(\boldsymbol{\omega}, \eta)$  are  $Y$ -periodic, representing the displacements in the entire solid part,  $Y_{m*} = Y_m \cup Y_*$  and the electric potential in the matrix part  $Y_m$ .

We shall use the bilinear forms (24) with obvious modifications, namely  $g_Y^m(\cdot, \cdot)$  and  $d_Y^m(\cdot, \cdot)$  involve the coefficients  $\bar{g}_{kij}$  and  $\bar{d}_{kl}$ , respectively, see (39).

The local microstructural response is obtained by solving the following decoupled problems:

- Find  $(\boldsymbol{\omega}^{ij}, \hat{\eta}^{ij}) \in \mathbf{H}_{\#}^1(Y_{m*}) \times H_{\#0*}^1(Y_m)$  for any  $i, j = 1, 2, 3$  satisfying

$$\begin{aligned} a_Y^{m*}(\boldsymbol{\omega}^{ij} + \boldsymbol{\Pi}^{ij}, \mathbf{v}) - g_Y^m(\mathbf{v}, \hat{\eta}^{ij}) &= 0, \quad \forall \mathbf{v} \in \mathbf{H}_{\#}^1(Y_{m*}), \\ g_Y^m(\boldsymbol{\omega}^{ij} + \boldsymbol{\Pi}^{ij}, \psi) + d_Y^m(\hat{\eta}^{ij}, \psi) &= 0, \quad \forall \psi \in H_{\#0*}^1(Y_m), \end{aligned} \quad (48)$$

- Find  $(\boldsymbol{\omega}^P, \hat{\eta}^P) \in \mathbf{H}_{\#}^1(Y_{m*}) \times H_{\#0*}^1(Y_m)$  satisfying

$$\begin{aligned} a_Y^{m*}(\boldsymbol{\omega}^P, \mathbf{v}) - g_Y^m(\mathbf{v}, \hat{\eta}^P) &= - \int_{\Gamma_c} \mathbf{v} \cdot \mathbf{n}^{[c]} \, dS_y, \quad \forall \mathbf{v} \in \mathbf{H}_{\#}^1(Y_m), \\ g_Y^m(\boldsymbol{\omega}^P, \psi) + d_Y^m(\hat{\eta}^P, \psi) &= 0, \quad \forall \psi \in H_{\#0*}^1(Y_m), \end{aligned} \quad (49)$$

- Find  $(\boldsymbol{\omega}^\rho, \hat{\eta}^\rho) \in \mathbf{H}_\#^1(Y_{m^*}) \times H_{\#0^*}^1(Y_m)$  satisfying

$$\begin{aligned} a_Y^{m^*}(\boldsymbol{\omega}^\rho, \mathbf{v}) - g_Y^m(\mathbf{v}, \hat{\eta}^\rho) &= 0, \quad \forall \mathbf{v} \in \mathbf{H}_\#^1(Y_m), \\ g_Y^m(\boldsymbol{\omega}^\rho, \psi) + d_Y^m(\hat{\eta}^\rho, \psi) &= \int_{\Gamma_{mc}} \psi \, dS_y, \quad \forall \psi \in H_{\#0^*}^1(Y_m), \end{aligned} \quad (50)$$

- Find  $(\hat{\boldsymbol{\omega}}^k, \hat{\varphi}^k) \in \mathbf{H}_\#^1(Y_{m^*}) \times H_{\#0,k}^1(Y_m)$  satisfying, for  $k = 1, 2, \dots, k^*$ ,

$$\begin{aligned} a_Y^{m^*}(\hat{\boldsymbol{\omega}}^k, \mathbf{v}) - g_Y^m(\mathbf{v}, \hat{\varphi}^k) &= 0, \quad \forall \mathbf{v} \in \mathbf{H}_\#^1(Y_m), \\ g_Y^m(\hat{\boldsymbol{\omega}}^k, \psi) + d_Y^m(\hat{\varphi}^k, \psi) &= 0, \quad \forall \psi \in H_{\#0^*}^1(Y_m). \end{aligned} \quad (51)$$

#### 4.4. Macroscopic model

We pursue the analogous procedure reported in Section 3.4. As the consequence of the convergence result related to the two-scale potential  $\hat{\varphi}^0(x, y)$ , the limit problem is defined in terms of  $\mathbf{u}^0$  and  $p^0$  only: Find  $\mathbf{u}^0 \in \mathcal{U}(\Omega)$  and  $p^0 \in L^2(\Omega)$  such that

$$\begin{aligned} &\int_{\Omega} e_{ij}^x(\mathbf{v}^0) [a_Y^{m^*}(\mathbf{u}^1 - \boldsymbol{\Pi}^{kl} e_{kl}^x(\mathbf{u}^0), \boldsymbol{\Pi}^{ij}) - g_Y^m(\boldsymbol{\Pi}^{ij}, \hat{\varphi}^0)] \, dV_x \\ &\quad - \int_{\Omega} p^0 \phi \nabla_x \cdot \mathbf{v}^0 \, dV_x = \int_{\Omega} \hat{\mathbf{f}} \cdot \mathbf{v}^0 \, dV_x + \int_{\partial\Omega} \mathbf{h} \cdot \mathbf{v}^0 \, dS_x, \quad (52) \\ &\int_{\Omega} q^0 \left( \phi \nabla_x \cdot \mathbf{u}^0 - \int_{\Gamma_c} \mathbf{u}^1 \cdot \mathbf{n}^{[m^*]} \, dS_y \right) \, dV_x + \gamma \int_{\Omega} \phi p^0 q^0 \, dV_x = 0, \end{aligned}$$

for all  $(\mathbf{v}^0, q^0) \in \mathcal{U}_0(\Omega) \times L^2(\Omega)$ . By  $\hat{\mathbf{f}} = \int_{Y_{m^*}} \mathbf{f}$  the average volume forces are denoted.

Using the characteristic responses (48)–(51) obtained at the microscopic scale, upon substituting the split form of the two-scale functions (47) into (52), the homogenized coefficients can be computed in analogy with the treat-



ment explained in Section 3.

$$\begin{aligned}
A_{klij}^H &= a_Y^{m*} (\boldsymbol{\omega}^{ij} + \boldsymbol{\Pi}^{ij}, \boldsymbol{\Pi}^{kl}) - g_Y^m (\boldsymbol{\Pi}^{kl}, \hat{\eta}^{ij}) \\
&= a_Y^{m*} (\boldsymbol{\omega}^{ij} + \boldsymbol{\Pi}^{ij}, \boldsymbol{\omega}^{kl} + \boldsymbol{\Pi}^{kl}) + d_Y^m (\hat{\eta}^{kl}, \hat{\eta}^{ij}) , \\
B_{ij}^H &= a_Y^{m*} (\boldsymbol{\omega}^P, \boldsymbol{\Pi}^{ij}) - g_Y^m (\boldsymbol{\Pi}^{ij}, \hat{\eta}^P) + \phi \delta_{ij} = - \int_{Y_m} \nabla_y \cdot \boldsymbol{\omega}^{ij} dV_y + \phi \delta_{ij} , \\
H_{ij}^k &= a_Y^{m*} (\hat{\boldsymbol{\omega}}^k, \boldsymbol{\Pi}^{ij}) - g_Y^m (\boldsymbol{\Pi}^{ij}, \hat{\varphi}^k) , \\
S_{ij}^H &= a_Y^{m*} (\boldsymbol{\omega}^\rho, \boldsymbol{\Pi}^{ij}) - g_Y^m (\boldsymbol{\Pi}^{ij}, \hat{\eta}^\rho) , \\
R^H &= - \int_{\Gamma_c} \boldsymbol{\omega}^\rho \cdot \mathbf{n}^{[c]} dS_y , \\
M^H &= \int_{\Gamma_c} \boldsymbol{\omega}^P \cdot \mathbf{n}^{[c]} dS_y + \phi \delta_{ij} = a_Y^{m*} (\boldsymbol{\omega}^P, \boldsymbol{\omega}^P) + d_Y^m (\hat{\eta}^P, \hat{\eta}^P) + \phi \delta_{ij} , \\
Z^k &= - \int_{\Gamma_c} \hat{\boldsymbol{\omega}}^k \cdot \mathbf{n}^{[c]} dS_y .
\end{aligned} \tag{53}$$

We can now rewrite (52) in terms of the coefficients (53), thus, the macroscopic problem for the DFC\* reads: Find  $\mathbf{u}^0 \in \mathbf{U}(\Omega)$  and  $p^0 \in L^2(\Omega)$  such that

$$\begin{aligned}
\int_{\Omega} \mathbf{e}(\mathbf{v}^0) : (\mathbb{A}^H \mathbf{e}(\mathbf{u}^0) - p \mathbf{B}^H) dV_x &= - \int_{\Omega} \mathbf{e}(\mathbf{v}^0) : \left( \sum_k \mathbf{H}^k \bar{\varphi}^k + \mathbf{S}^H \rho_E \right) dV_x \\
&\quad + \int_{\Omega} \hat{\mathbf{f}} \cdot \mathbf{v}^0 dV_x + \int_{\partial\Omega} \bar{\mathbf{h}}(\bar{p}) \cdot \mathbf{v}^0 dS_x , \\
\int_{\Omega} q^0 (\mathbf{B}^H : \mathbf{e}(\mathbf{u}^0) + p M^H) dV_x &= \int_{\Omega} q^0 \left( \sum_k Z^k \bar{\varphi}^k + R^H \rho_E \right) dV_x ,
\end{aligned} \tag{54}$$

for all  $\mathbf{v}^0 \in \mathbf{U}_0(\Omega)$  and for all  $q^0 \in L^2(\Omega)$ .

The homogenized piezoelectric material obeys the poroelastic law with the poroelastic coefficients modified due to the piezoelectric effect. The imposed voltage, *i.e.* the potentials prescribed on the distributed conductors, and the interface charges generate a prestress which, upon integrating by parts, can be presented in terms of volume forces.

Analogous procedure pursued for the case DFC\*S leads to the same poroelastic model, however, since the fluid inclusions are disconnected,  $\bar{Y}_c \subset Y$ , the

macroscopic pressure  $p(x)$  depends on  $x$ . To simplify the notation, in what follows we drop the superscripts  $^0$  in all macroscopic variables. In analogy with (35) and (36), the differential form of (54) is presented by the following equations, dropping the superscripts  $^0$ :

$$\begin{aligned} -\nabla \cdot \boldsymbol{\sigma}^H(\mathbf{u}, p) &= \hat{\mathbf{f}}, & \text{in } \Omega, \\ \boldsymbol{\sigma}^H(\mathbf{u}, p) \cdot \mathbf{n} &= \bar{\mathbf{h}}, & \text{on } \partial_\sigma \Omega, \end{aligned} \quad (55)$$

with the constitutive equations:

$$\begin{aligned} \boldsymbol{\sigma}^H(\mathbf{u}, p) &= \mathbb{A}^H \mathbf{e}(\mathbf{u}) - p \mathbf{B}^H + \sum_k \mathbf{H}^k \bar{\varphi}^k + \mathbf{S}^H \rho_E, \\ p &= \frac{1}{M^H} \left( \sum_k Z^k \bar{\varphi}^k + R^H \rho_E - \mathbf{B}^H : \mathbf{e}(\mathbf{u}) - j \right), \end{aligned} \quad (56)$$

where  $j = J/|\Omega|$  has been introduced in (36) assuming the connected porosity; for disconnected fluid-saturated inclusions we put  $j = 0$  in (56). From (56)<sub>1</sub>, the pressure can be eliminated, so that the “undrained” coefficients can be obtained in analogy with (38).

**Remark 4.1.** *Both the models, as presented in Sections 3 and 4 can be adapted easily for the other type of the porosity, thus, the form of the macroscopic constitutive equations can be deduced easily also for cases CFC\* and DFD\*. If the porosity is connected, the models can be extended for fluid flow problems; for this, the pressure is considered as a scalar field  $p(x)$  and, in (36) and (56), we put  $j = \nabla \cdot \mathbf{w}$ , where, denoting by  $\mathbf{v}^f$  the mean fluid velocity,  $\mathbf{w} = \phi(\mathbf{v}^f - \dot{\mathbf{u}})$  is the seepage velocity governed by the Darcy flow law  $\mathbf{w} = -\bar{\eta}^{-1} \mathbf{K} \nabla p$  involving the fluid viscosity. As far as the quasistatic problems are considered, cf. [23], the permeability can be obtained for a specific geometry by the standard homogenization of the Stokes flow, see e.g. [25].*

## 5. Problem formulation for the homogenized media

To allow for more general situations of loading the deforming piezoporoelastic media, we shall generalize the homogenization results obtained above for the two different cases of heterogeneous media by considering more general boundary conditions. To introduce them for the coupled problem, we need the following two decompositions of  $\partial\Omega$  into disjoint parts:

$$\begin{aligned} \partial\Omega &= \partial_\sigma \Omega \cup \partial_u \Omega, & \partial_\sigma \Omega \cap \partial_u \Omega &= \emptyset, \\ \partial\Omega &= \partial_E \Omega \cup \partial_\varphi \Omega, & \partial_E \Omega \cap \partial_\varphi \Omega &= \emptyset. \end{aligned} \quad (57)$$

The displacement and the electric potential must satisfy the boundary conditions which will now be specified for the two homogenized models derived above.

### 5.1. Model CFD\*

We consider the following boundary conditions, where  $D_n$  and  $\mathbf{g}^s$  are given:

$$\begin{aligned} \mathbf{u} &= \mathbf{0} & \text{on } \partial_u \Omega, & & \mathbf{n} \cdot \boldsymbol{\sigma} &= \mathbf{g}^s & \text{on } \partial_\sigma \Omega, \\ \varphi &= \bar{\varphi}^0 & \text{on } \partial_\varphi \Omega, & & \mathbf{n} \cdot \vec{D} &= D_n & \text{on } \partial_E \Omega. \end{aligned} \quad (58)$$

The parts  $\partial_u \Omega$  and  $\partial_\varphi \Omega$  are nonvanishing, therefore, the admissibility sets  $\mathbf{U}(\Omega)$ ,  $\mathcal{V}(\Omega)$  introduced in Section 3.4 along with the associated spaces of test functions  $\mathbf{U}_0(\Omega)$ ,  $\mathcal{V}_0(\Omega)$  are considered. In the *drained* case, pressure  $\bar{p}$  is given. Consequently, since equation (34)<sub>3</sub> can be released, the formulation (34) is reduced. In the *undrained* case, pressure  $\bar{p}$  must be computed, thus, the formulation (34) applies. For the numerical tests reported below in Section 7,  $D_n = 0$  and  $\mathbf{g}^s = 0$ .

### 5.2. Model DFC\*

In this case, part  $\partial_\varphi \Omega$  vanishes, so that (58) is modified: we consider  $\mathbf{n} \cdot \vec{D} = D_n$  on the whole  $\partial \Omega$ . The voltage  $\bar{\varphi}^k$ ,  $k = 1, 2$  is prescribed and the formulation (54) is employed.

## 6. Reconstruction of the solutions at the microscopic level

In this section we provide formulae which enable to reconstruct displacement, pressure and velocity fields at the level of the heterogeneity's. This procedure is affected by a given finite scale  $\varepsilon_0 > 0$ .

First we introduce the so-called folding procedure. The two-scale field reconstruction is based on the coordinate split related to the periodic lattice. For  $\varepsilon_0 > 0$ , using the rescaled cell  $Z^{\varepsilon_0} = \varepsilon_0 Y$  we introduce its local copies  $Z^{K, \varepsilon_0}$  labeled by index  $K$  whereby  $\{\bar{x}^K\}_K$  is the set of centers of each  $Z^{K, \varepsilon_0}$ . For the sake of simplicity, we consider only such domains  $\Omega$  which are generated as a union of non overlapping RVEs  $Z^{K, \varepsilon_0}$ , thus (recall that  $\bar{Z}$  is the closure of  $Z$ )

$$\bar{\Omega} = \bigcup_{K \in \Xi_\Omega^{\varepsilon_0}} \bar{Z}^{K, \varepsilon_0}, \quad Z^{K, \varepsilon_0} = Z^{\varepsilon_0} + \boldsymbol{\xi}^K, \quad (59)$$

where  $\Xi_{\Omega}^{\varepsilon_0}$  is the set of indices  $K$  associated to the lattice vector  $\mathbf{k} = (k_i) \in \mathbb{Z}^3$  such that  $\boldsymbol{\xi}^K = \varepsilon_0 k_i a_i$ , recalling the definition  $Y = \prod_i ] - a_i/2, a_i/2[$ .

For any global position  $x \in Z^{K, \varepsilon_0}$ , the local “mesoscopic” coordinate

$$y = (x - \bar{x}^K)/\varepsilon_0, \quad (60)$$

can be introduced, such that  $y \in Y$ . Then any two-scale function  $f(x, y)$  can be evaluated by combining the macroscopic responses, such as displacements  $\mathbf{u}^0(x)$ ,  $x \in \Omega$ , and by the local “autonomous” characteristic responses. Although, at this point, we must distinguish between the two models described in the preceding sections, the folding procedure can be summarized, as follows: for each “real sized” cell  $Y^{K, \varepsilon_0}$  with its center  $\bar{x}^K$  evaluate the local responses given below as two-scale functions  $f(x, y)$ , where  $x \in Z^{K, \varepsilon_0}$  and  $y \in Y$  is given by (60).

### 6.1. Reconstruction for the CFD\* model

As the basis for reconstruction of the microscopic strains and the electric field, the convergence result (19) and the split (23) of the fluctuating fields  $\mathbf{u}^1, \varphi^1$  must be interpreted for a given size of the microstructure, thus, for a given  $\varepsilon_0 > 0$ . This allows us to evaluate approximations of  $\mathbf{u}^{R\varepsilon_0}$  and  $\varphi^{R\varepsilon_0}$  by virtue of (21). When dealing with the numerical implementation, an interpolation of the macroscopic fields  $\mathbf{e}_x(\mathbf{u}^0)$  and  $\nabla_x \varphi^0$  must be used to introduce continuous two-scale functions  $f(x, y)$  at the global level for  $x \in \Omega$ , and  $y \in Y$  associated with  $x$  by (60). In particular, we can introduce the Q1 interpolation scheme of the finite element method with interpretation of the lattice formed by copies  $Z^{K, \varepsilon_0}$ ; let  $\mathcal{Z}_{\varepsilon_0}(\Omega)$  be such “element partitioning”. By  $\tilde{g}$  we denote the projection of a given function  $g(x)$  in the space of piecewise Q1 polynomials defined over  $\mathcal{Z}_{\varepsilon_0}(\Omega)$ .

Now, recalling (21), we can express the reconstructed fields  $\mathbf{u}^{R\varepsilon_0}, \varphi^{R\varepsilon_0}$  using the approximated two-scale functions,

$$\begin{aligned} \mathbf{u}^{1, \varepsilon_0}(x, y) &:= \boldsymbol{\omega}^{ij}(y) \widetilde{e_{ij}^x(\mathbf{u}^0)} + \boldsymbol{\omega}^k(y) \widetilde{\partial_k^x \varphi^0} - \bar{p}^0 \boldsymbol{\omega}^P(y), \\ \varphi^{1, \varepsilon_0}(x, y) &:= \eta^{ij}(y) \widetilde{e_{ij}^x(\mathbf{u}^0)} + \eta^k(y) \widetilde{\partial_k^x \varphi^0} - \bar{p}^0 \eta^P(y), \end{aligned} \quad (61)$$

where  $\bar{p}^0(x) = \bar{p}$  is the macroscopic pressure. When dealing with disconnected inclusions,  $\bar{p}^0(x)$  corresponds to the pressure in  $Z^{K, \varepsilon}$  of the particular local RVE. Consequently, the convergence result on the gradients yields the

strain and the electric fields approximations,

$$\begin{aligned}\mathbf{e}^{\text{mic}}(x, y) &= \widetilde{\mathbf{e}_x(\mathbf{u}^0)} + \mathbf{e}_y(\mathbf{u}^{1, \varepsilon_0}), \\ \nabla \varphi^{\text{mic}} \equiv \vec{E}^{\text{mic}}(x, y) &= \widetilde{\nabla_x \varphi^0} + \nabla_y \varphi^{1, \varepsilon_0},\end{aligned}\tag{62}$$

which can be rewritten in terms of the local response gradients:

$$\begin{aligned}\mathbf{e}^{\text{mic}}(x, y) &= \widetilde{\mathbf{e}_x(\mathbf{u}^0)} + \mathbf{e}_y(\boldsymbol{\omega}^{ij}) \widetilde{e_{ij}^x(\mathbf{u}^0)} + \mathbf{e}_y(\boldsymbol{\omega}^k) \widetilde{\partial_k^x \varphi^0} - \mathbf{e}_y(\boldsymbol{\omega}^P) \bar{p}^0, \\ \vec{E}^{\text{mic}}(x, y) &= \widetilde{\nabla_x \varphi^0} + \nabla_y \eta^{ij} \widetilde{e_{ij}^x(\mathbf{u}^0)} + \nabla_y \eta^k \widetilde{\partial_k^x \varphi^0} - \nabla_y \eta^P \bar{p}^0.\end{aligned}\tag{63}$$

It should be noted that (62)<sub>1</sub> and (62)<sub>2</sub> can be extended naturally by terms  $\varepsilon_0 \mathbf{e}_x(\mathbf{u}^{1, \varepsilon_0})$  and  $\varepsilon_0 \nabla_x \varphi^{1, \varepsilon_0}$ , respectively.

### 6.2. Reconstruction for the DFC\* model

In this case, the reconstruction of the microscopic strains and the electric field follows the analogous guidelines as those explained above for the CFD\* model. Therefore, we only describe the major differences. Importantly, the computational material parameters  $\bar{\mathbf{g}}$  and  $\bar{\mathbf{d}}$  must be defined for a given  $\varepsilon_0$  using (39), where  $\underline{\mathbf{g}}^{\varepsilon_0}$  and  $\underline{\mathbf{d}}^{\varepsilon_0}$  present the right physical values.

For the reconstruction of displacements  $\mathbf{u}^{R\varepsilon_0}$  and  $\varphi^{R\varepsilon_0}$ , in (45), the relevant two-scale functions are expressed according to the decomposed form (47) modified due to the projection of the macroscopic strains into the Q1 polynomial bases associated with the partitioning  $\mathcal{Z}_{\varepsilon_0}(\Omega)$  introduced in the preceding section. Thus, since  $\varrho_E$  and  $\bar{\varphi}^k$  are assumed continuous (or even constant) functions in  $x$ , (47) yields:

$$\begin{aligned}\mathbf{u}^{1, \varepsilon_0}(x, y) &= \boldsymbol{\omega}^{ij}(y) \widetilde{e_{ij}^x(\mathbf{u}^0)} - p^0(x) \boldsymbol{\omega}^P(y) + \boldsymbol{\omega}^\rho(y) \rho_E + \sum_k \hat{\boldsymbol{\omega}}^k(y) \bar{\varphi}^k, \\ \varphi^{0, \varepsilon_0}(x, y) &= \hat{\eta}^{ij}(y) \widetilde{e_{ij}^x(\mathbf{u}^0)} - p^0(x) \hat{\eta}^P(y) + \hat{\eta}^\rho(y) \rho_E + \sum_k \hat{\varphi}^k(y) \bar{\varphi}^k.\end{aligned}\tag{64}$$

Then the convergence result on the gradients, see (43)<sub>2,4</sub> yields the strain and the electric fields approximations,

$$\begin{aligned}\mathbf{e}^{\text{mic}}(x, y) &= \widetilde{\mathbf{e}_x(\mathbf{u}^0)} + \mathbf{e}_y(\mathbf{u}^{1, \varepsilon_0}), \\ \nabla \varphi^{\text{mic}} \equiv \vec{E}^{\text{mic}}(x, y) &= \frac{1}{\varepsilon_0} \nabla_y \varphi^{0, \varepsilon_0},\end{aligned}\tag{65}$$

where the substitutions due to (64) are obvious. Beyond the first order approximation, (65)<sub>1</sub> and (65)<sub>2</sub> can be extended naturally by terms  $\varepsilon_0 \mathbf{e}_x(\mathbf{u}^{1, \varepsilon_0})$  and  $\nabla_x \varphi^{0, \varepsilon_0}$ , respectively; note the difference with the CFD\* model.

## 7. Numerical examples

In this section we demonstrate two-scale modelling of the porous piezoelectric media using the two homogenized models described above. The numerical simulations presented in this section has been performed in *SfePy* – Simple Finite Elements in Python, see [26]. It is a software for solving multiscale systems of coupled partial differential equations by means of the finite element method. Both the models, CFD\* and DFC\*, have been implemented in this software, whereby the displacements and the electric potential were approximated by piecewise three-linear functions, thus, the Q1 hexahedral elements are employed. For the model DFC\* with fluid inclusions the pressure is approximated by the piecewise constant functions.

### 7.1. Validation test: homogenization vs. reference model

To validate the proposed homogenized model of fluid-saturated piezoelectric porous media, we rely on the numerical results obtained by direct simulations of the heterogeneous periodic structure. Thus, the reference numerical model is established by copies  $Z^{K,\varepsilon_0}$  of the reference cell  $Z^{\varepsilon_0}$ , as discussed in Section 6. To capture accurately effects related to the microstructure geometry, highly refined finite element meshes associated with all cells  $Z^{K,\varepsilon_0}$  are required for a given size  $\varepsilon_0 > 0$ . For the validation test we consider the homogenized model DFC\* featured by disconnected fluid inclusions and connected conductor fibers. The local problems (48)–(51) are solved in the unit cell  $Y$  represented by the rescaled finite element mesh. Responses computed by the macroscopic model represented by (53), (54) are compared to the responses of the poroelastic-piezoelectric reference model which is defined by the equilibrium equations (5), (6), and by interface and boundary conditions (9) and (10). In this section, we use subscripts  $x, y, z$  to refer to the coordinate axes directions, thus, we write  $u_y$  instead of  $u_2$ , etc.

We consider a block sample of dimensions  $0.01 \times 0.01\varepsilon_0 \times 0.01$  m on which we apply the following boundary conditions:  $u_y = 0$  at the bottom face, see Fig.2 right,  $u_x = 0$  at the left face and the periodic condition in  $y$  direction (front and back faces). No volume and surface forces and surface electric charge are considered, thus,  $\hat{\mathbf{f}} = \mathbf{0}$ ,  $\bar{\mathbf{h}} = \mathbf{0}$ ,  $\varrho_E = 0$  in (54). The piezoelectric matrix is made of barium–titanite BaTiO<sub>3</sub>, see Tab. 1 for its material properties, the properties of metallic conductors are given by Young’s modulus  $E = 200$  GPa and Poisson’s ration  $\nu = 0.25$ , and the fluid compressibility is  $4.651 \times 10^{-10}$  Pa.

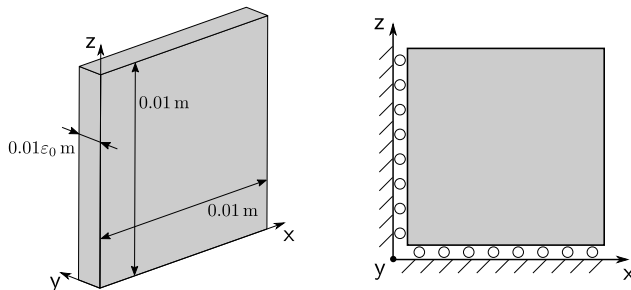


Figure 2: Sample used in the validation test: left – shape and dimensions of the sample; right – applied boundary conditions,  $u_y = 0$  at the bottom face,  $u_x = 0$  at the left face, periodic conditions in  $y$  direction at the front and back faces.

elasticity (in GPa):	$A_{1111}$	$A_{3333}$	$A_{1122}$	$A_{2233}$	$A_{1313}$	$A_{1212}$
	15.040	14.550	6.560	6.590	4.240	4.390
piezo-coupling (in C/m <sup>2</sup> ):	$g_{311}$	$g_{322}$	$g_{333}$	$g_{223}$		
	-4.322	-4.322	17.360	11.404		
dielectricity (in 10 <sup>-8</sup> C/Vm):	$d_{11}$	$d_{33}$				
	1.284	1.505				

Table 1: Piezoelectric properties of the porous matrix. The transverse isotropy yields the following symmetries:  $A_{2233} = A_{1133}$ ,  $A_{1313} = A_{2323}$ ,  $g_{311} = g_{322}$ ,  $g_{223} = g_{113}$ ,  $d_{11} = d_{22}$ . Other components are zero.

The homogenized response is obtained by solving separately the macroscopic and the microscopic problems; the corresponding domains  $\Omega$  and  $Y$  for these subproblems are depicted in Fig. 3 top. The finite element mesh used in the reference model is build up as an array of cells  $Z^{K,\varepsilon_0}$ , by repeating the representative cell  $Z^{\varepsilon_0}$  in the  $x$  and the  $z$  directions, see Fig. 3 top-right and bottom. The number of copies in these two directions is referred as a “grid” in the subsequent text and figures. There are no external loads prescribed, so that the deformation of the sample is induced due to the piezoelectric effect, as the response to the locally prescribed potentials  $\bar{\varphi}^1 = +1000$  V and  $\bar{\varphi}^2 = -1000$  V associated with the two conductors. In the case of the reference model, these potentials are applied as the interface conditions, see (9), while in the homogenized model they appear at the r.h.s. of (54).

The responses of the reference model are shown in Fig. 4 left, where the fluid pressure in the inclusions, strain field and electric field are depicted. The right part of Fig. 4 shows the relative error of the fields calculated by

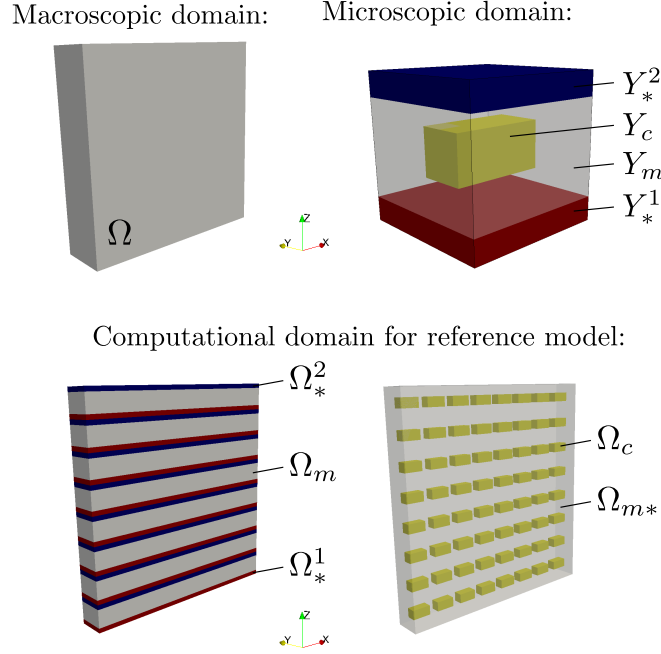


Figure 3: Computational domains: top – macroscopic domain  $\Omega$  (left) and decomposition of microscopic domain  $Y$  (right); bottom – domain use in the reference model build up by repetition of the microscopic unit.

the homogenized model. The strain and electric fields are reconstructed according to (64), (65), whereby the homogenized fluid pressure results from macroscopic equations (54). The relative error for the pressure, strains, and the electric field displayed in the figure is defined as  $f_{err} = |f^{dir} - f^{hom}|/f^{dir}$ , where  $f$  stands for  $p$ ,  $\|e\|$  and  $\|\vec{E}\|$ , respectively. In Fig. 5, fluid pressures and displacements  $u_x, u_z$  along line  $\bar{l}$  are compared. The biggest differences apparent near the right and top borders of the sample appear there because the periodicity assumption applied in the homogenized model is not satisfied at this boundary. When moving to the left bottom part, where symmetric boundary conditions are applied, the boundary effect vanishes and the relative difference drops significantly. Figure 6 shows how the relative pressure error is decreasing with the increasing grid number, i.e.  $\varepsilon_0 \rightarrow 0$ .

For the reference model, the solution time of the validation test with  $\varepsilon_0 = 0.01/\text{grid}$ , where  $\text{grid} = 24$ , is about 300 seconds and the finite element model has approximately  $4.5 \times 10^5$  degrees of freedom (DOFs). For the



corresponding homogenized medium, the solution time is about 20 seconds including reconstructions of the fields at a given macroscopic element, which take the most amount of the computational time. The microscopic problems with 741 DOFs are solved several times to compute all the corrector functions, then the macroscopic problem with 577 DOFs is solved.

### 7.2. DFC\* example

As in the preceding section, we consider the isolated fluid inclusions and two continuous conductors embedded in the piezoelectric matrix, see Fig. 7 right. The left face of the macroscopic sample, with dimensions  $0.01 \times 0.0025 \times 0.01$  m, is attached to the rigid wall, see Fig. 7 left, the periodic boundary condition is applied in  $y$  direction and the deformation is induced by prescribing potentials  $\pm 1000$  V in the embedded conductors. The deformed shape (deformation scaled by factor 300) of the sample and pressure field  $p$  and the magnitude of macroscopic strain  $\mathbf{e}(\mathbf{u}^0)$  are depicted in Fig. 8. The reconstructed strain and electric fields for  $\varepsilon_0 = 0.01/64$  (grid = 64) at a given macroscopic element are shown in Fig. 9.

### 7.3. CFD\* example

In this part, we present the numerical simulation of the piezoelectric medium with connected fluid channels governed by equations (25)–(27) and (29)–(34). For the sake of simplicity the structure without conductor inclusions is considered. We omit them because they are passive elements only, contrary to the previous examples. The sample is again fixed on its left face, the periodic condition is applied in  $y$  direction and the deformation is now invoked by the prescribed electrical potentials at the bottom and top face of the sample, see Fig. 10 left,  $\bar{\varphi}^1 = -1000$  V,  $\bar{\varphi}^2 = +1000$ . The fluid pressure,  $\bar{p}$  in (34), is constant in the whole macroscopic domain and can be treated either as a unknown variable in the case when the fluid pores are closed on the outer surface (impermeable boundary) – undrained case, or as a given value determined by the pressure of a surrounding medium – drained case.

The macroscopic responses and reconstructed strain and electric fields for the undrained case are depicted in Figs. 11, 12. The computed homogenized coefficients  $\mathbf{B}^H$ ,  $M^H$ ,  $\mathbf{F}^H$  and  $\mathbb{A}^H$ ,  $\underline{\mathbf{G}}^H$ ,  $\mathbf{D}^H$  are summarized in Tables 2 and 3, where  $\mathbb{A}^H$ ,  $\underline{\mathbf{G}}^H$ ,  $\mathbf{D}^H$  are compared to the material properties of the homogeneous solid skeleton. The finite size of the microstructure is given by  $\varepsilon_0 = 0.01/64$ .

$B_{11}^H$	$B_{33}^H$	$M^H$	$F_3^H$
0.347	0.370	$4.834 \times 10^{-121}$ Pa	$-4.464 \times 10^{-12}$ m/V

Table 2: Homogenized coefficients  $\mathbf{B}^H$ ,  $M^H$ ,  $\mathbf{F}^H$ .

elasticity (in $10^{10}$ Pa):	$A_{1111}^H$	$A_{3333}^H$	$A_{1122}^H$	$A_{2233}^H$	$A_{1313}^H$	$A_{1212}^H$
homogen. prop.	9.745	7.888	2.582	2.376	3.452	3.114
skeleton prop.	15.040	14.550	6.560	6.590	4.240	4.390
piezo-coupling (in C/m <sup>2</sup> ):	$G_{311}^H$	$G_{322}^H$	$G_{333}^H$	$G_{223}^{H*}$		
homogen. prop.	-1.484	-1.142	11.348	5.761		
skeleton prop.	-4.322	-4.322	17.360	11.404		
dielectricity (in $10^{-8}$ C/Vm):	$D_{11}^H$	$D_{33}^H$				
homogen. prop.	0.997	0.988				
skeleton prop.	1.284	1.505				

Table 3: Homogenized piezoelectric coefficients  $\mathbb{A}^H$ ,  $\underline{\mathbf{G}}^H$ ,  $\mathbf{D}^H$  compared to the properties of the homogeneous piezoelectric material.

## 8. Conclusion

We considered heterogeneous periodic microstructure consisting of a piezo-electric skeleton with embedded conducting parts and penetrated by channels filled with a electrically neutral fluid. Using the the homogenization method we derived macroscopic models of the fluid saturated porous piezoelectric material. We elaborated two models for different topologies of the pores and arrangements of metallic conducting parts.

The model CFD\* is characterized by a single connected porosity, whereas the metal parts can be distributed as small inclusions. The obtained effective constitutive law for the stress and the electric displacement involves new coefficients related to the pore fluid pressure. As the consequence, by increasing the fluid pressure, or the pore fluid volume, the electric field can be generated, whereby the inverse effect appears, being naturally consistent with Onsager reciprocity principles. The macroscopic model derived by upscaling from the level of heterogeneities is consistent with the phenomenological models, cf. [18, 17].

The periodic structure for model DFC\* is characterized by fluid inclusions embedded in the piezoelectric matrix and by two, or more metallic electrodes being embedded in the matrix. In the latter case, an external elec-

tric field is imposed through given electric potentials associated with each of the electrodes. This electric field intensity blows up with  $\varepsilon^{-1}$  when  $\varepsilon \rightarrow 0$ , *i.e.* decreasing the microstructure characteristic size. To compensate the effect, a weakly piezoelectric material must be considered; the coupling and the dielectricity constants of the skeleton piezoelectric material are scaled proportionally to the microstructure size  $\varepsilon$ , so that the limit macroscopic model could be obtained. The obtained model describes a metamaterial with an interesting property of locally controllable pore fluid pressure. This option will be pursued further to develop a model of fluid transport controllable by voltage distributed by means of electrodes penetrating into the periodic medium structure.

For both the models we presented the microscopic level response reconstruction which is based on the characteristic responses and the macroscopic solutions of the particular problem. This was employed to validate the homogenized medium models. As the reference model for the validation, we used the direct numerical finite element simulation of a given periodic heterogeneous piezoelectric material interacting with the fluid.

*Acknowledgment.* This research is supported by project GACR 16-03823S and in part by project LO 1506 of the Czech Ministry of Education, Youth and Sports.

## Appendix A

We prove the symmetry relationships (33). The first equality (33)<sub>1</sub> follows from (27) and (26),

$$\begin{aligned} \int_{Y_m} \nabla_y \cdot \boldsymbol{\omega}^i dV_y &= a_Y^{m*}(\boldsymbol{\omega}^P, \boldsymbol{\omega}^i) - g_Y^m(\boldsymbol{\omega}^i, \eta^P) \\ &= g_Y^m(\boldsymbol{\omega}^P, \eta^i + y_i) + d_Y^m(\eta^i + y_i, \eta^P) = g_Y^m(\boldsymbol{\omega}^P, y_i) + d_Y^m(y_i, \eta^P) . \end{aligned} \quad (66)$$

To show (33)<sub>2</sub>, we employ (25) and (26), which yields:

$$\begin{aligned} -a_Y^{m*}(\boldsymbol{\omega}^k, \boldsymbol{\Pi}^{ij}) &= a_Y^{m*}(\boldsymbol{\omega}^{ij}, \boldsymbol{\omega}^k) - g_Y^m(\boldsymbol{\omega}^k, \eta^{ij}) , \\ g_Y^m(\boldsymbol{\Pi}^{ij}, \eta^k) &= d_Y^m(\eta^{ij}, \eta^k) - g_Y^m(\boldsymbol{\omega}^{ij}, \eta^k) \\ &= d_Y^m(\eta^{ij}, y_k) + g_Y^m(\boldsymbol{\omega}^k, \eta^{ij}) + g_Y^m(\boldsymbol{\omega}^{ij}, y_k) - a_Y^{m*}(\boldsymbol{\omega}^k, \boldsymbol{\omega}^{ij}) . \end{aligned} \quad (67)$$

Upon summation the above two equalities the equality (33)<sub>2</sub> follows. In analogy, to show (33)<sub>3</sub>, we employ (25) and (27); the following equalities

$$\begin{aligned}
a_Y^{m*}(\boldsymbol{\omega}^P, \boldsymbol{\Pi}^{ij}) &= a_Y^{m*}(\boldsymbol{\omega}^{ij}, \boldsymbol{\omega}^P) - g_Y^m(\boldsymbol{\omega}^P, \eta^{ij}) \\
&= d_Y^m(\eta^P, \eta^{ij}) + g_Y^m(\boldsymbol{\omega}^{ij}, \eta^P) + \int_{\Gamma_Y} \boldsymbol{\omega}^{ij} \cdot \mathbf{n}^{[m]} dS_y, \quad (68) \\
g_Y^m(\boldsymbol{\Pi}^{ij}, \eta^P) &= -d_Y^m(\eta^{ij}, \eta^P) - g_Y^m(\boldsymbol{\omega}^{ij}, \eta^P).
\end{aligned}$$

Upon summation the above two equalities the equality (33)<sub>3</sub> follows.

The symmetric expressions of  $\mathbb{A}^H = (A_{ijkl}^H)$  and  $\mathbf{D}^H = (D_{kl}^H)$  are obtained due to the local problems (25) and (26). Obviously, the tensors  $\mathbb{A}^H = (A_{ijkl}^H)$ , and  $\mathbf{B}^H = (B_{ij}^H)$  are symmetric,  $\mathbb{A}^H$  inherits all the symmetries of  $\mathbb{A}$ ; moreover  $\mathbb{A}$  is positive definite and  $M^H > 0$ .

## References

- [1] G. Ayuso, M. Friswell, S. Adhikari, H. Khodaparast, H. Berger, Homogenization of porous piezoelectric materials, *Int. J. Solids Struct.* 113–114 (2017) 218–229. doi:10.1016/j.ijsolstr.2017.03.003.
- [2] E. Sanchez-Palencia, Non-homogeneous media and vibration theory, no. 127 in *Lecture Notes in Physics*, Springer, Berlin, 1980.
- [3] D. Cioranescu, P. Donato, An introduction to homogenization, no. 17 in *Oxford Lecture Series in Mathematics and its Applications*, Oxford University Press, Oxford, 1999.
- [4] G. Allaire, Homogenization and two-scale convergence, *SIAM J. Math. Anal.* 23 (1992) 1482–1518. doi:10.1137/0523084.
- [5] D. Cioranescu, A. Damlamian, G. Griso, The periodic unfolding method in homogenization, *SIAM J. Math. Anal.* 40 (4) (2008) 1585–1620. doi:10.1137/080713148.
- [6] F. Fantoni, A. Bacigalupo, M. Paggi, Multi-field asymptotic homogenization of thermo-piezoelectric materials with periodic microstructure, *Int. J. Solids Struct.* 120 (2017) 31–56. doi:10.1016/j.ijsolstr.2017.04.009.

- [7] B. Miara, E. Rohan, M. Zidi, B. Labat, Piezomaterials for bone regeneration design-homogenization approach, *J. Mech. Phys. Solids* 53 (11) (2005) 2529–2556. doi:10.1016/j.jmps.2005.05.006.
- [8] V. Sikavitsas, J. Temenoff, A. Mikos, Biomaterials and bone mechanotransduction, *Biomaterials* 22 (19) (2001) 2581–2593. doi:10.1016/S0142-9612(01)00002-3.
- [9] H.-P. Wiesmann, M. Hartig, U. Stratmann, U. Meyer, U. Joos, Electrical stimulation influences mineral formation of osteoblast-like cells in vitro, *BBA-Mol. Cell Res.* 1538 (1) (2001) 28–37. doi:10.1016/S0167-4889(00)00135-x.
- [10] S. Iyer, T. Venkatesh, Electromechanical response of (3–0, 3–1) particulate, fibrous, and porous piezoelectric composites with anisotropic constituents: A model based on the homogenization method, *Int. J. Solids Struct.* 51 (6) (2014) 1221–1234. doi:10.1016/j.ijsolstr.2013.12.008.
- [11] J. Viaño, C. Ribeiro, J. Figueiredo, A. Rodríguez-Arós, A high order model for piezoelectric rods: An asymptotic approach, *Int. J. Solids Struct.* 81 (2016) 294–310. doi:10.1016/j.ijsolstr.2015.12.005.
- [12] E. Rohan, B. Miara, Homogenization and shape sensitivity of microstructures for design of piezoelectric bio-materials, *Mech. Adv. Mater. Struc.* 13 (6) (2006) 473–485. doi:10.1080/15376490600862848.
- [13] Y. Koutsawa, S. Belouettar, A. Makradi, H. Nasser, Sensitivities of effective properties computed using micromechanics differential schemes and high-order taylor series: Application to piezo-polymer composites, *Mech. Res. Commun.* 37 (5) (2010) 489–494. doi:10.1016/j.mechrescom.2010.06.001.
- [14] J. J. Telega, R. Wojnar, Flow of electrolyte through porous piezoelectric medium: macroscopic equations, *C. R. Acad. Sci. Paris, Série II b* 328 (2000) 225–230. doi:10.1016/S1287-4620(00)00121-6.
- [15] T. Lemaire, E. Capiez-Lernout, J. Kaiser, S. Naili, E. Rohan, V. Sansalone, A multiscale theoretical investigation of electric measurements in

- living bone. piezoelectricity and electrokinetics, *B. Math. Biol.* 73 (11) (2011) 2649–2677. doi:10.1007/s11538-011-9641-9.
- [16] V. Levin, T. Michelitsch, H. Gao, Propagation of electroacoustic waves in the transversely isotropic piezoelectric medium reinforced by randomly distributed cylindrical inhomogeneities, *Int. J. Solids Struct.* 39 (19) (2002) 5013–5051. doi:10.1016/S0020-7683(02)00401-8.
- [17] A. Vashishth, V. Gupta, Wave propagation in transversely isotropic porous piezoelectric materials, *Int. J. Solids Struct.* 46 (20) (2009) 3620–3632. doi:10.1016/j.ijsolstr.2009.06.011.
- [18] M. D. Sharma, Piezoelectric effect on the velocities of waves in an anisotropic piezo-poroelastic medium, *Proc. R. Soc. A* 466 (2010) 1977–1992. doi:10.1098/rspa.2009.0534.
- [19] A. Vashishth, V. Gupta, Reflection and transmission of plane waves from a fluid-porous piezoelectric solid interface, *J. Acoust. Soc. Am.* 129 (6) (2011) 3690–3701. doi:10.1121/1.3586792.
- [20] J. P. Besombes, C. Gagnolati, M. Lagier, Low-frequency cutoff in fluid-saturated porous piezoelectric ceramics, *J. Acoust. Soc. Am.* 88 (S1). doi:10.1121/1.2028618.
- [21] E. Rohan, S. Naili, T. Lemaire, Double porosity in fluid-saturated elastic media: deriving effective parameters by hierarchical homogenization of static problem, *Continuum Mech. Therm.* 28 (5) (2015) 1263–1293. doi:10.1007/s00161-015-0475-9.
- [22] E. Rohan, V. Lukeš, On modelling nonlinear phenomena in deforming heterogeneous media using homogenization and sensitivity analysis concepts, *Appl. Math. Computat.* 267 (2015) 583–595. doi:10.1016/j.amc.2015.01.054.
- [23] E. Rohan, S. Shaw, J. Whiteman, Poro-viscoelasticity modelling based on upscaling quasistatic fluid-saturated solids, *Computat. Geosci.* 18 (5) (2013) 883–895. doi:10.1007/s10596-013-9363-1.
- [24] D. Brown, P. Popov, Y. Efendiev, On homogenization of stokes flow in slowly varying media with applications to fluid-structure interaction, *Int. J. Geomath.* 2 (2) (2011) 281–305. doi:10.1007/s13137-011-0025-y.

- [25] U. Hornung, Homogenization and porous media, Springer, 1997.
- [26] R. Cimrman, SfePy - write your own FE application, in: P. de Buyl, N. Varoquaux (Eds.), Proceedings of the 6th European Conference on Python in Science (EuroSciPy 2013), 2014, pp. 65–70, <http://arxiv.org/abs/1404.6391>.

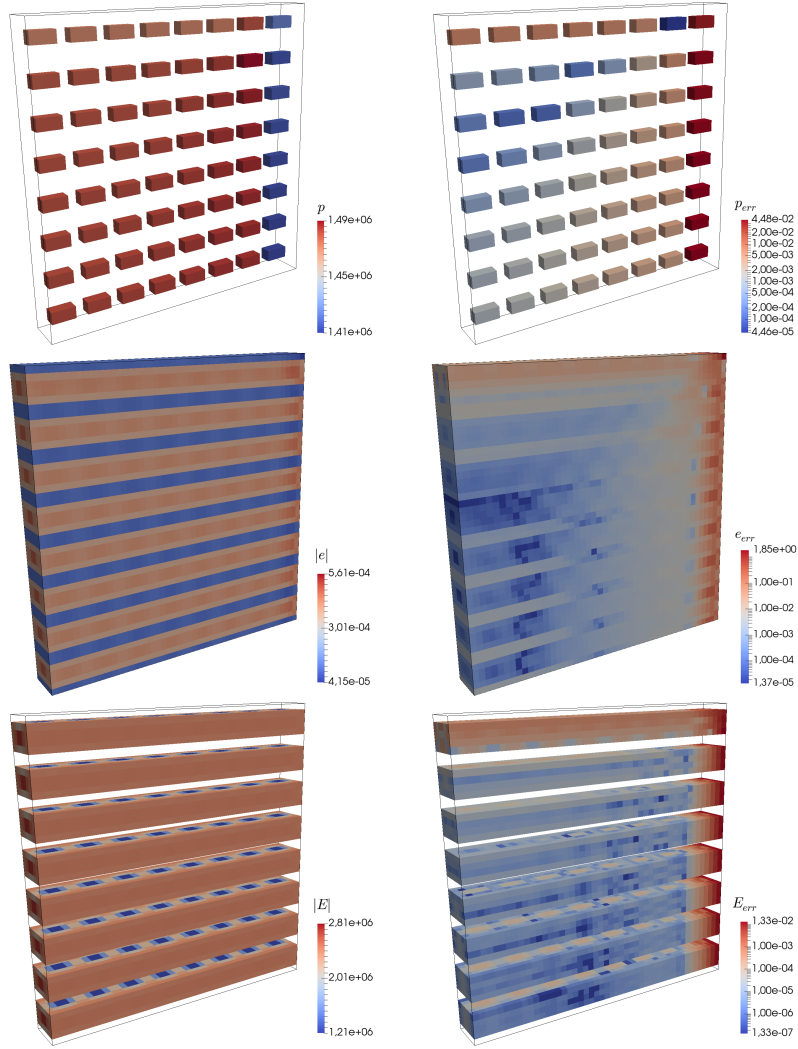


Figure 4: Left – responses of the reference model: fluid pressure  $p$ , strain field magnitude  $\|\mathbf{e}\|$ , electric field magnitude  $\|\vec{E}\|$ ; right – relative errors of the results obtained by the homogenized model.



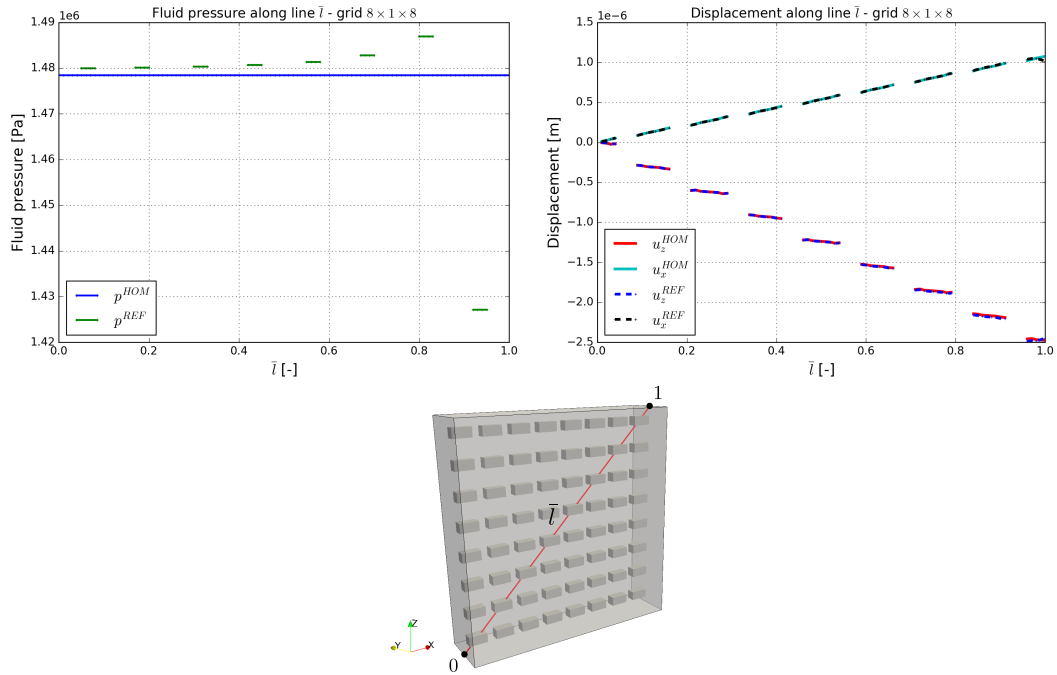


Figure 5: Responses of the homogenized and reference model over line  $\bar{l}$ : left – fluid pressure; right – displacements  $u_x, u_z$ .

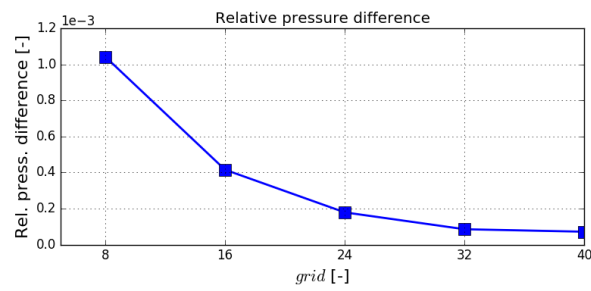


Figure 6: Drop of the relative pressure error with the increasing grid number.

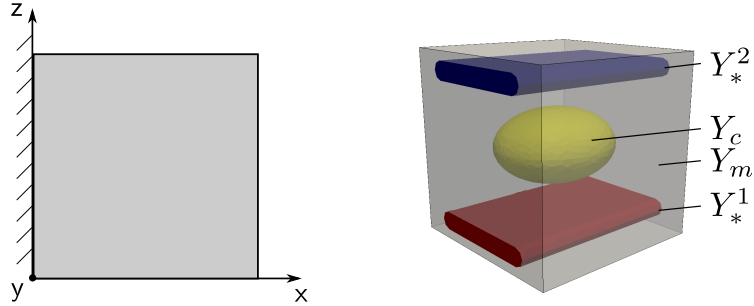


Figure 7: Left – boundary conditions applied at the macroscopic level; right – geometry of the DFC\* microscopic periodic cell (RVE).

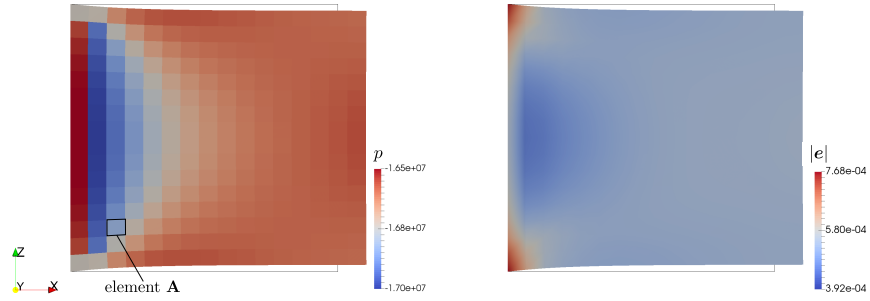


Figure 8: Deformed macroscopic (displacements scaled by factor 300) sample and the resulting fields, DFC\* model: left – pressure  $p$ ; right – magnitude of macroscopic strain  $e(\mathbf{u}^0)$ .

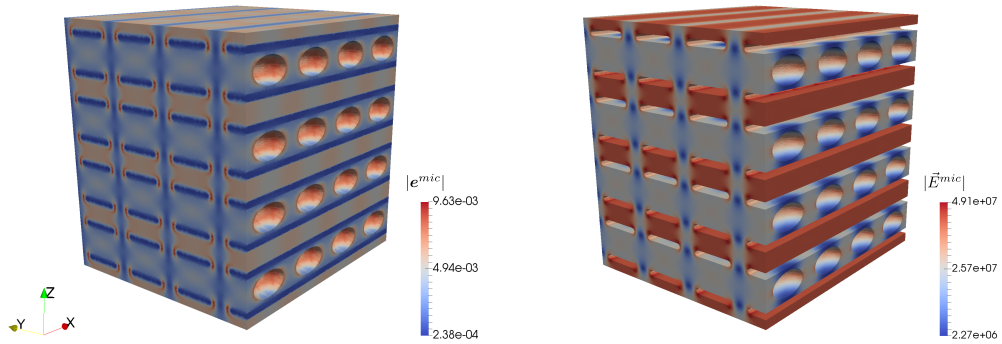


Figure 9: Magnitudes of reconstructed fields at the macroscopic element **A** (see Fig. 8), DFC\* model: left – strain field  $e^{mic}$ ; right – electric field  $\vec{E}^{mic}$ .

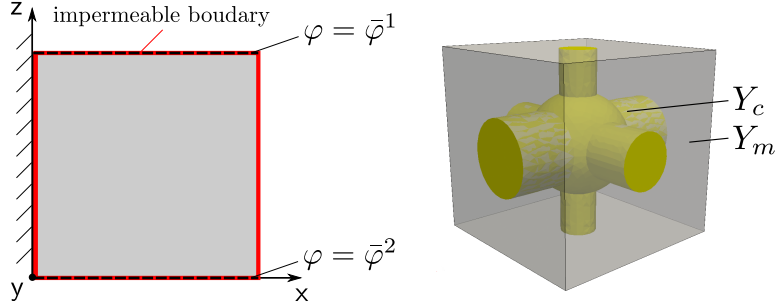


Figure 10: Left – boundary conditions applied at the macroscopic level; right – geometry of the CF(D\*) microscopic periodic cell (RVE).

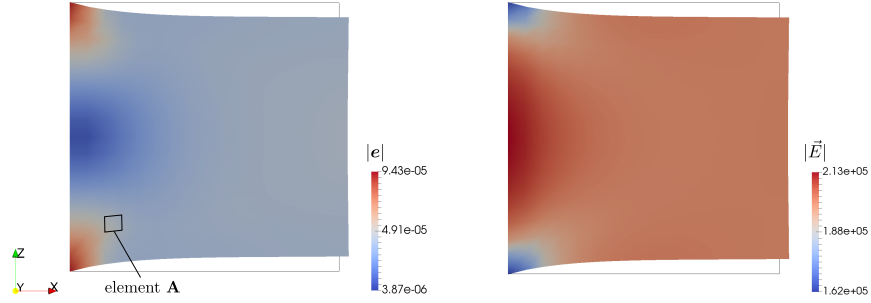


Figure 11: Deformed macroscopic (displacement scaled by factor 3000) sample and the resulting magnitudes of the macroscopic fields, CFD\* model: left – strain  $e(\mathbf{u}^0)$ ; right – macroscopic electric field  $\vec{E} = \nabla_x \varphi^0$ .

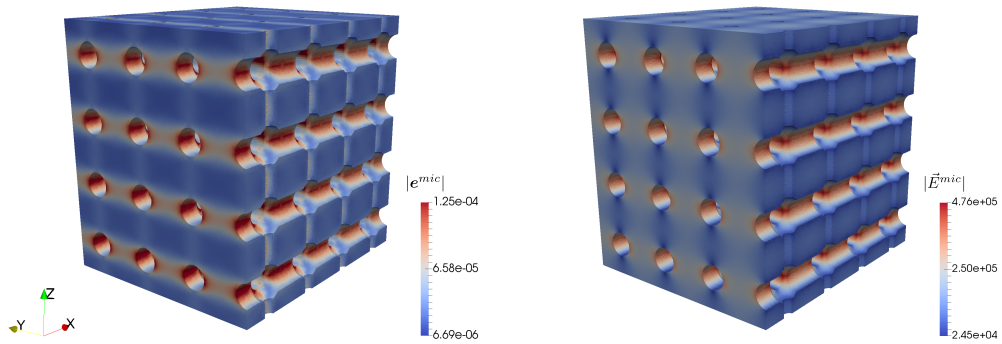


Figure 12: Magnitudes of reconstructed fields at the macroscopic element A (see Fig. 11), CFD\* model: left – strain field  $e^{mic}$ ; right – electric field  $\vec{E}^{mic}$ .